CANFSA

Center for Advanced Non-Ferrous Structural Alloys
An Industry/University Cooperative Research Center

# Project 36B-L: Compositional variations and finite element simulations of defects in AM Ti64

## Rationalization of Liquid/Solid and Solid/Solid Interface Instabilities During Thermal-Mechanical Transients of Metal Additive Manufacturing

## Semi-annual Spring Meeting

## April 2022


- ISU team: Katie O'Donnell, Amamchukwu Ilogebe, Maria Quintana
- Faculty: Dr. Peter Collins (ISU)
- MURI members: S. Babu (UTK), A. Clarke (CSM), J. R. Jinschek (OSU), T. Pollock (UCSB), Z. Kong (VT), S. Ringer and X. Liao (Univ. of Sydney), S. Primig (Univ. of South Wales) and TEAM
- Industrial Mentors: Billy Short and Jennifer Wolk (ONR)


COLORADO SCHOOL OF MINES

NSF

IOWA STATE UNIVERSITY

# Project 36B-L: Compositional variations and finite element simulations of defects in AM Ti64

## Rationalization of Liquid/Solid and Solid/Solid Interface Instabilities During Thermal-Mechanical Transients of Metal Additive Manufacturing

CANFSA
CENTER FOR ADVANCED NON-FERROUS STRUCTURAL ALLOYS

- ISU team: Katie O'Donnell, Amamchukwu Ilogebe, Maria Quintana
- Advisor(s): Prof. Peter Collins (ISU)

- Problem: Understand the thermal gradients in an AM build as a function of different scan strategies by studying the microstructure.
- Objective: To understand the science behind the relation between thermal gradients and the microstructure and texture evolution.
- Benefit: Optimize the final cost and mechanical properties of the AM component.

**Project Duration**
August 2018 to August 2021
Extended: August 2021 to August 2023

Recent Progress
- Compositional variations in AM
- Finite element simulations of defects in AM
- Preliminary microstructural analysis of Inconel 738 samples
- Preliminary microstructural analysis of Haynes 282 samples

| Metrics | | |
|---|---|---|
| **Description** | **% Complete** | **Status** |
| 1. Sample preparation for optical, SEM-BSE, EBSD and TEM | 75% | ● |
| 2. Literature review | 80% | ● |
| 3. Texture scans – EBSD, SRAS, and ASTAR PED | 65% | ● |
| 4. 3D analysis | 20% | ● |
| 5. Relate thermal gradients to microstructure and the final mechanical properties | 60% | ● |

# Industrial Relevance

- Understanding underlying behavior of different AM strategies on resulting microstructure and mechanical properties of metallic printed parts
- Build a scientific basis into Integrated Computational Materials Engineering (ICME) predictions of AM knowledge gap areas (nano and micro scale regimes of length and time)
- Reduce trial and error phase of AM design and manufacture curve

# Progress

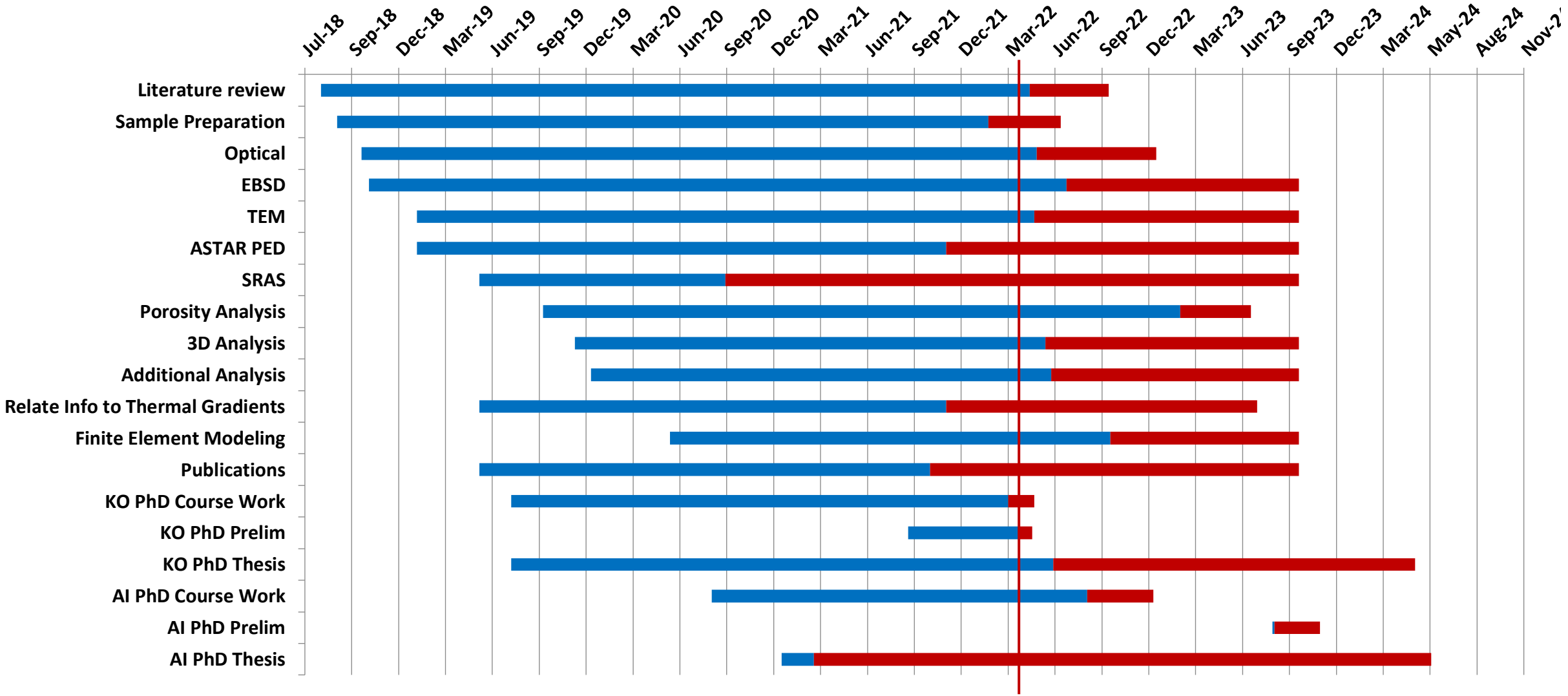

# Research Interests

Three different AM scan strategies are selected to understand fundamental research questions. The different scan strategies will change the thermal gradient: Raster, Dehoff, and Random

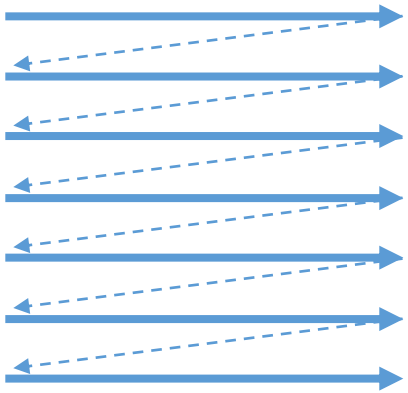

Ordering of Raster Fill

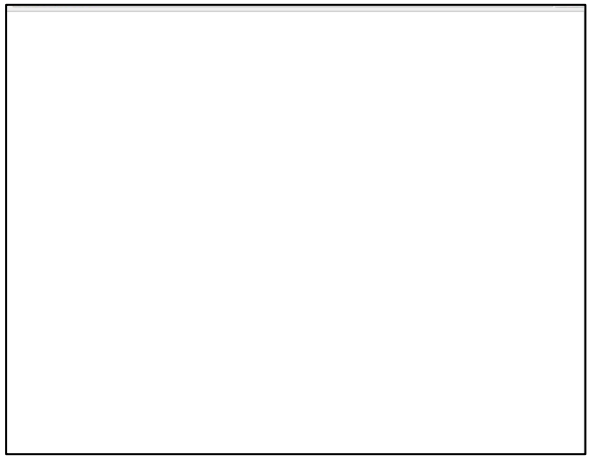

Ordering of Dehoff Fill

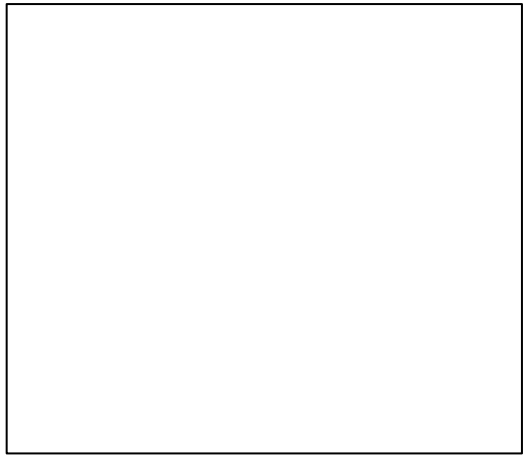

Ordering of Random Fill

# Outline of the Project

Ti64, Inconel 738, and Haynes 282 builds with different scan strategies and different geometries are provided by ORNL – Raster (L), Random (R), and Dehoff (D)

**TASKS:**

Imaging – Macro, Optical, and SEM-BSE

1. Texture (across length scales)
    A. SRAS – Spatially Resolved Acoustic Spectroscopy (macro-scale)
    B. EBSD – Electron Back Scattered Diffraction (SEM) (micro-scale)
    C. PED – Precession Electron Diffraction (TEM) (nano-scale)
2. Analysis of the 2D and 3D data
3. Develop the understanding to relate thermal gradient to the microstructural evolution

# Material

- 3 cuboid Ti64 builds – Raster (L5), Random (R5), and Dehoff (D5)
- 2 cuboid Inconel 738 builds – Random and Raster
- 3 Haynes 282 samples – pyramid, printed "pores" (cube, spiral)
- Z is the build direction for all the samples

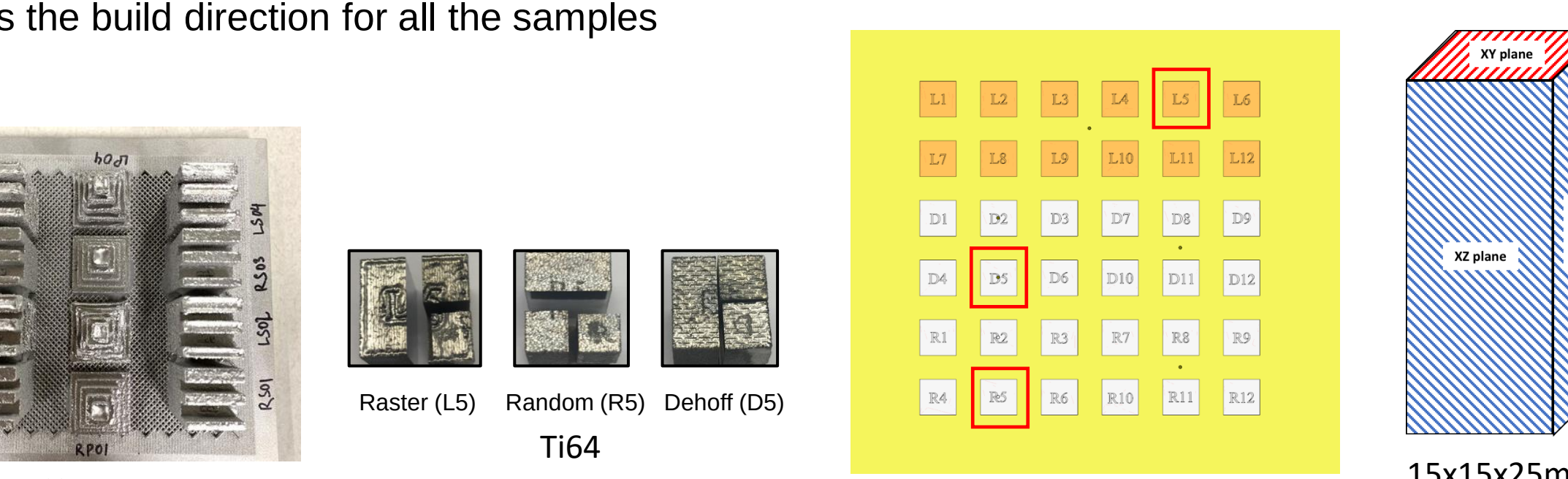




Haynes



Raster (L5) Random (R5) Dehoff (D5)

Ti64

15x15x25mm

# Outline

- Compositional variations in AM
  - Previous results
  - In the literature
  - Comparing AM processes, AM alloys, and AM scan strategies
- Finite Element Simulations of Defects in AM
  - Model introduction, “Stick Model” and “Layered Model”
  - CT data
  - Mimicking random defects
  - Preliminary Results for both models:
    - Tensile forces
    - Thermal forces
- Brief Inconel and Haynes microstructural analysis update

# Compositional Variations

# Local Compositional Variations

Previously, we have seen compositional variations across Ti64 scan strategies, in both EDS maps and through optical microscopy.

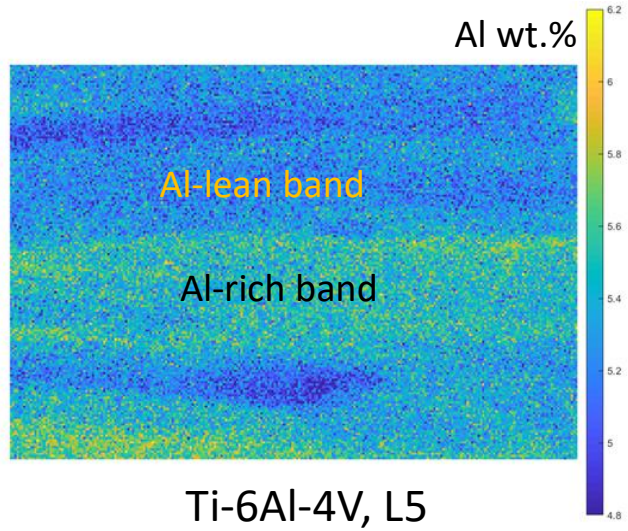


Ti-6Al-4V, L5

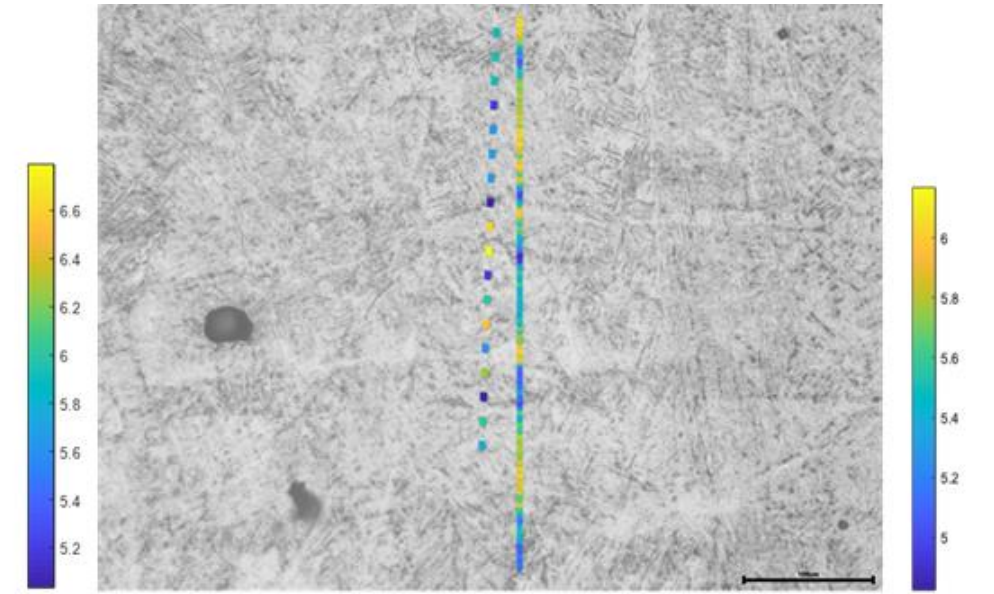


Hardness (GPa) Aluminum (wt%)

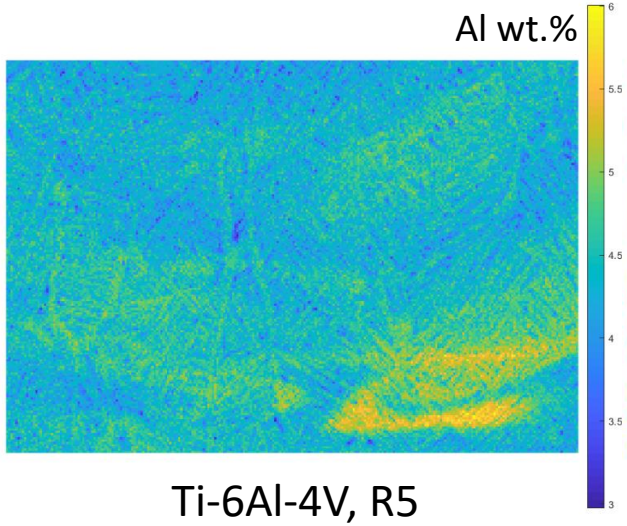


Ti-6Al-4V, R5

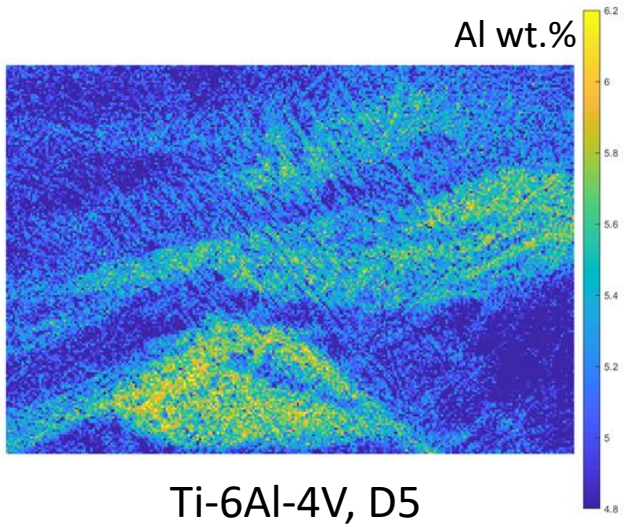


Ti-6Al-4V, D5

# Literature Review: Aluminum Vaporization

Electron beam cold-hearth melting of titanium alloys is known to be limited by poor compositional control.

Ideal evaporation can be governed by the Langmuir equation,

$$W_{Al}\ (kg/m^2 s) = P_{Al}[M_{Al}/(2\pi RT)]^{1/2}$$

where:

- $P_{Al}$ is the partial pressure of the vapor of Al (a function of molar fraction, activity coefficient, and vapor pressure above a melt of pure Al)
- $M_{Al}$ is the molar fraction
- $R$ is the gas constant
- $T$ is the temperature

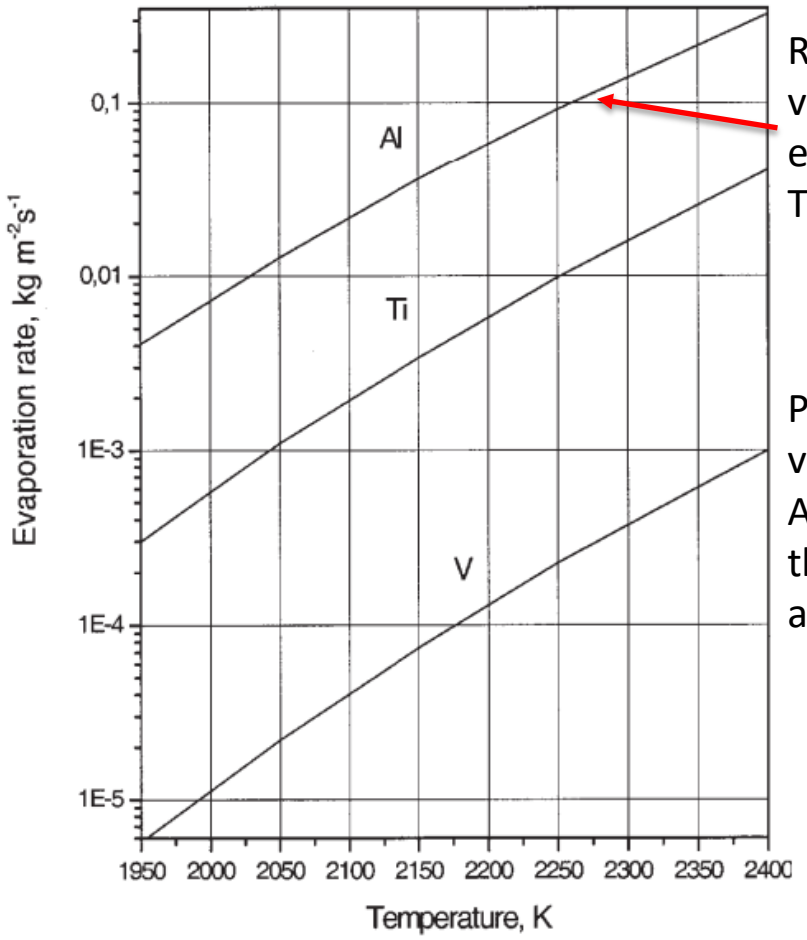


Rate of Al vaporization exceeds that of Ti or V

Preferential vaporization of Al in EBM is therefore likely as well

Ivanchenko, V. G., Ivasishin, O. M., & Semiatin, S. L. (2003). Evaluation of evaporation losses during electron-beam melting of Ti-Al-V alloys. *Metallurgical and Materials Transactions B*, *34*(6), 911-915.

# Literature Review: Aluminum Variations in AM Ti Alloys

EBM Ti-45Al-7Nb-0.3W alloy showing microstructural banding corresponding to aluminum variations

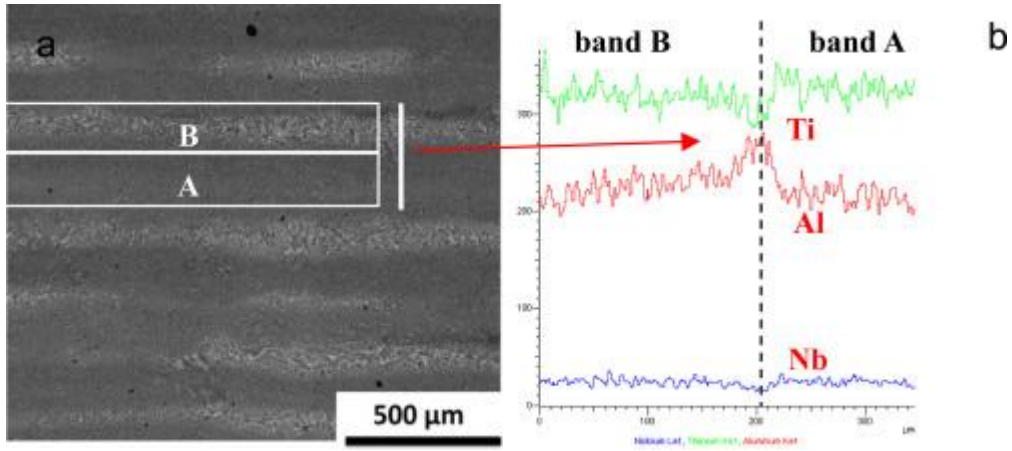


Tang, H. P., Yang, G. Y., Jia, W. P., He, W. W., Lu, S. L., & Qian, M. (2015). Additive manufacturing of a high niobium-containing titanium aluminide alloy by selective electron beam melting. Materials Science and Engineering: A, 636, 103-107.

EBM Ti-48Al-2Nb-2Cr alloy showing aluminum variations in all samples, while other elements (Nb) remain homogeneously distributed

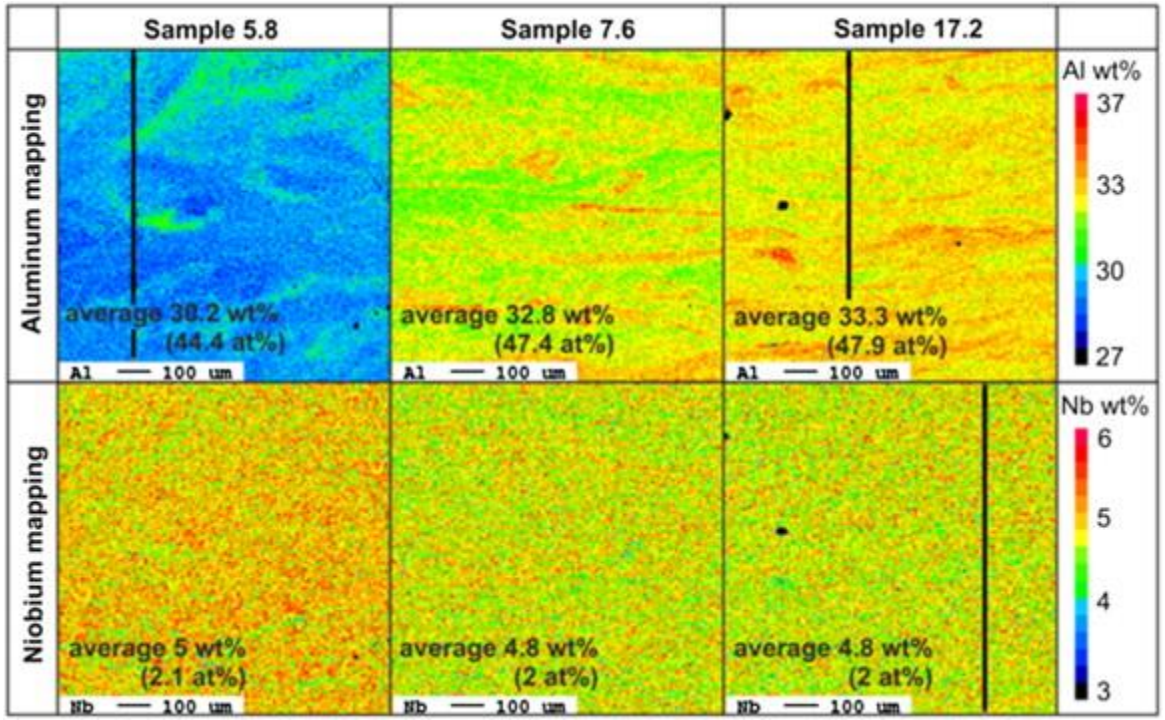


Schwerdtfeger, J., & Körner, C. (2014). Selective electron beam melting of Ti–48Al–2Nb–2Cr: Microstructure and aluminium loss. Intermetallics, 49, 29-35.

# Compositional Variations in Other AM Processes

No similar compositional inhomogeneity was observed in either the SLM or LHW Ti-6Al-4V samples.

The AM technique has a significant influence on the formation of microstructural banding and preferential aluminum vaporization.

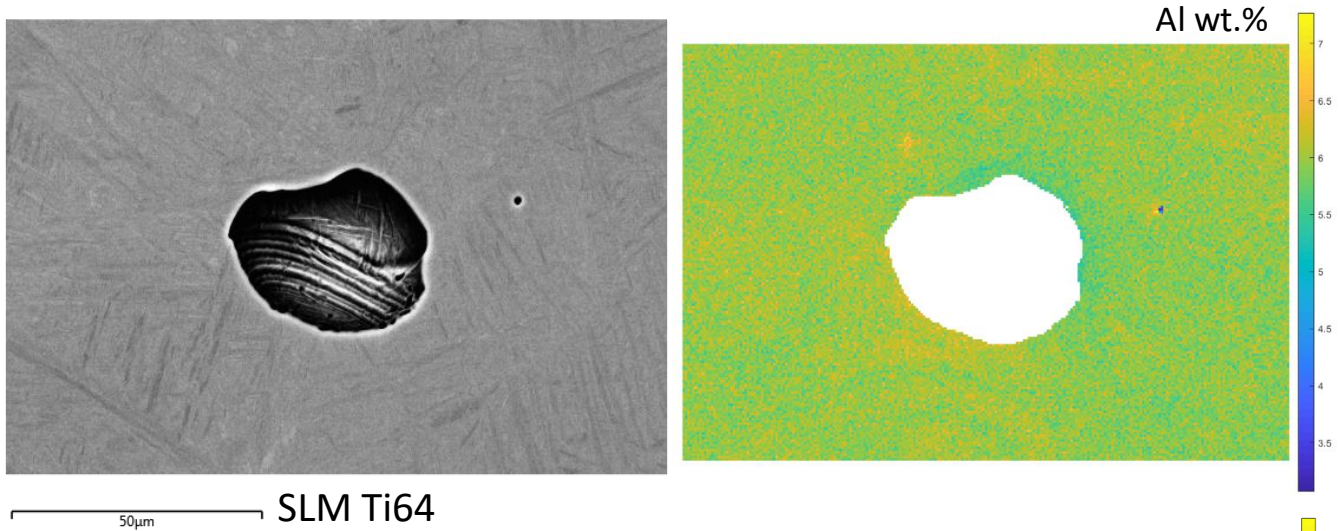


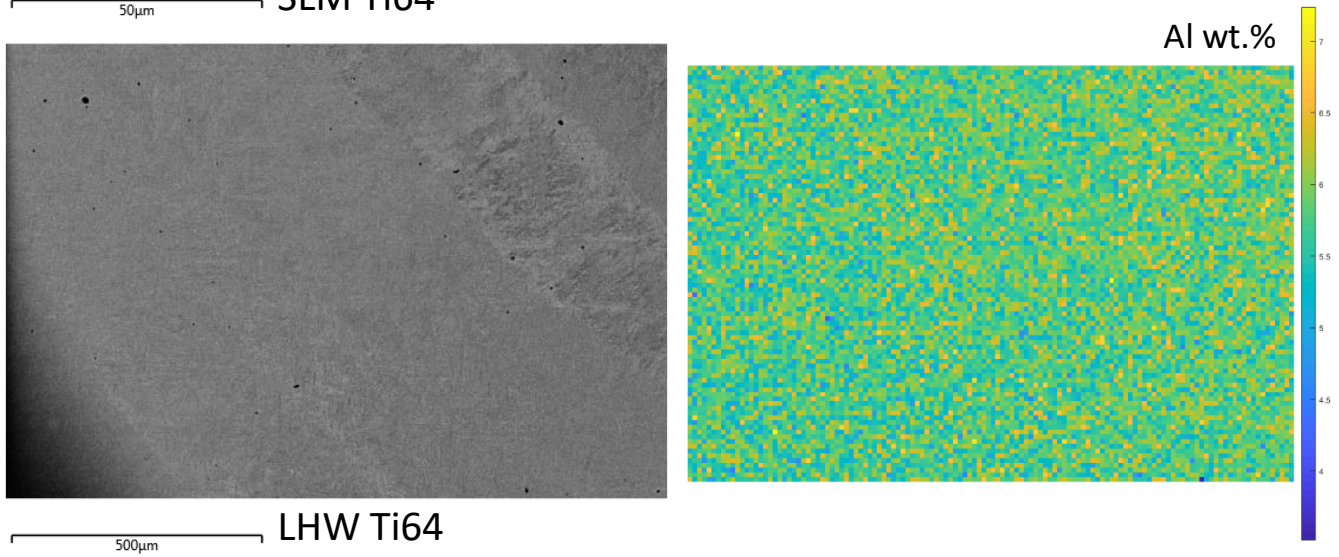

# Compositional Variations in other AM Alloys

No compositional variations were observed in MURI Inconel samples beyond those expected due to microstructural variations.

(i.e., no layer-by-layer vaporization)

Banding and preferential aluminum vaporization has thus far only been observed in MURI EBM Ti64.

MURI Inconel 738 (raster)

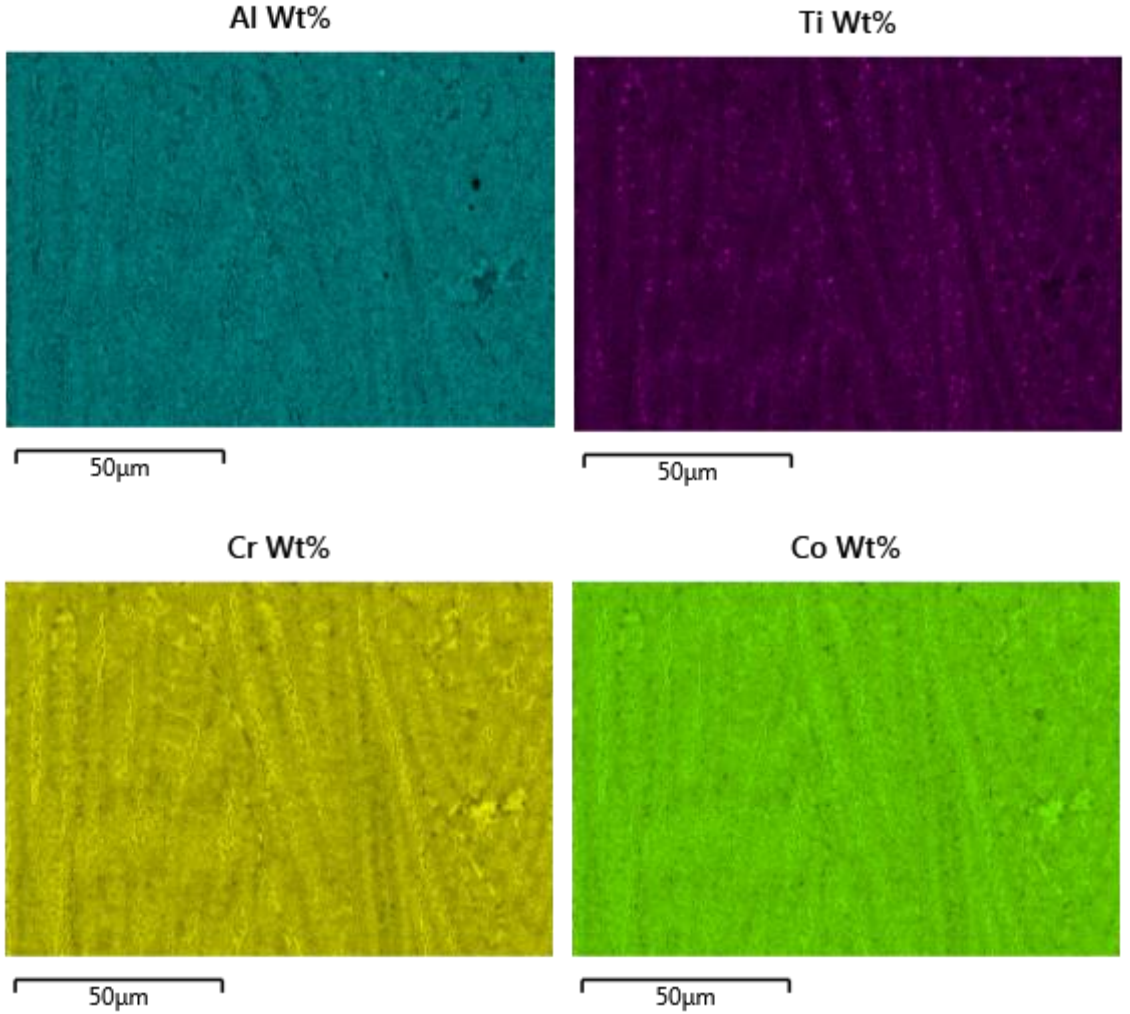

# Compositional Variations across AM Scan Strategies

Examining previous EDS maps again revealed a difference in aluminum content between scan strategies.

| | Al (wt.%) | |
|---|---|---|
| **L5** | | |
| **Average** | **5.49** | 9 maps |
| **St. Dev.** | **0.202** | |
| **R5** | | |
| **Average** | **4.63** | 2 maps |
| **St. Dev.** | **0.277** | |
| **D5** | | |
| **Average** | **4.97** | 2 maps |
| **St. Dev.** | **0.235** | |

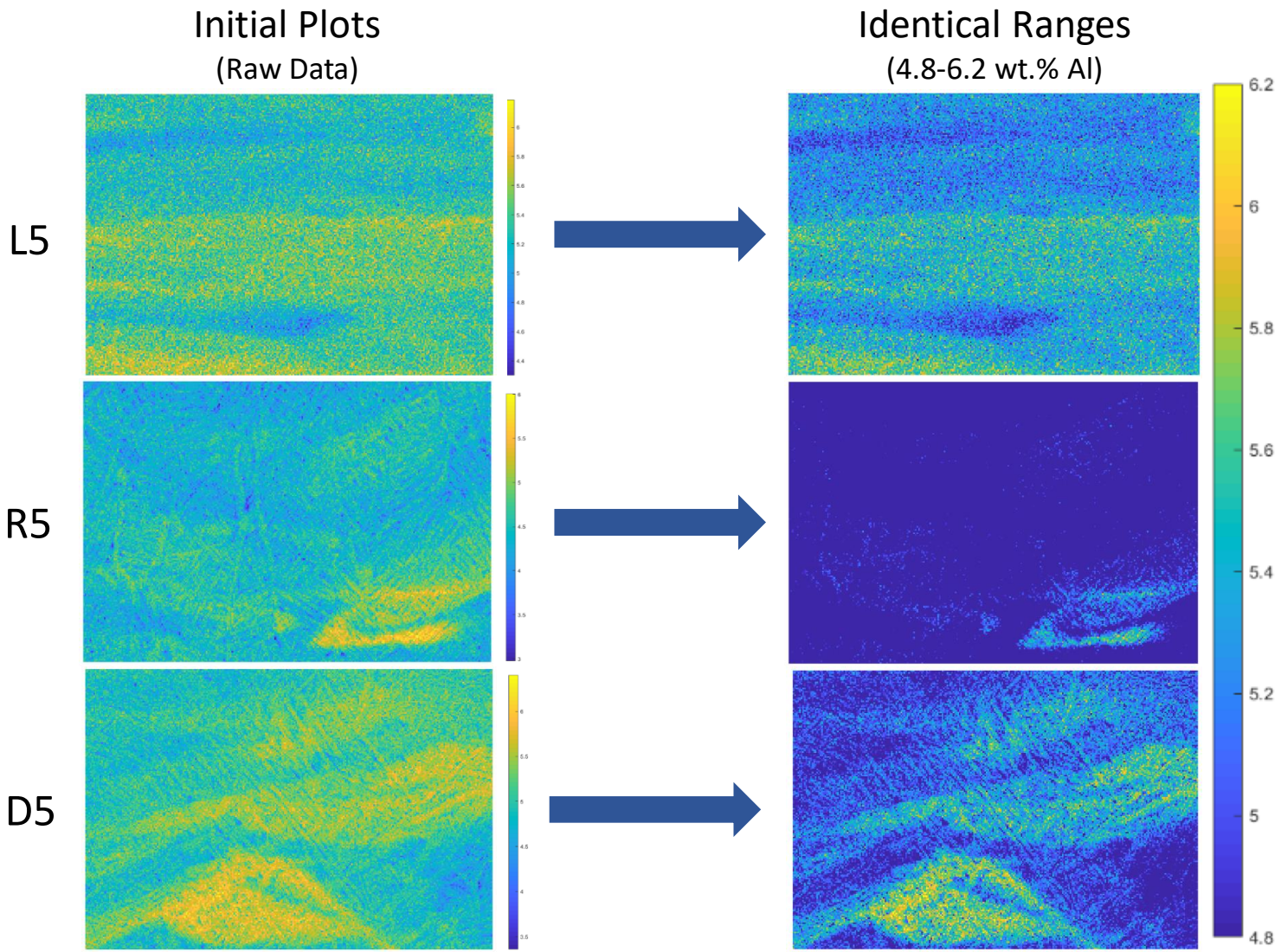

# Compositional Variations across AM Scan Strategies

Area EDS analyzes at 100x.

Same settings as previous maps.

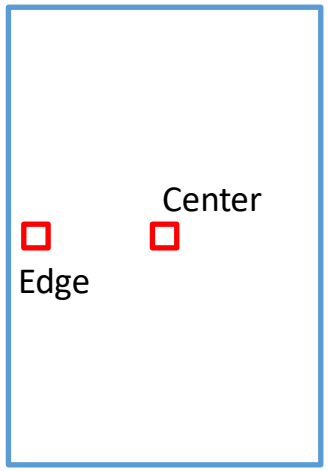


| | Ti | Al | V |
|---|---|---|---|
| **L5, Center** | 90.77 | 5.56 | 3.67 |
| **L5, Edge** | 90.81 | 5.51 | 3.68 |
| **R5, Center** | 91.66 | 4.57 | 3.77 |
| **R5, Edge** | 91.65 | 4.58 | 3.78 |
| **D5, Center** | 91.36 | 4.86 | 3.78 |
| **D5, Edge** | 91.48 | 4.74 | 3.78 |

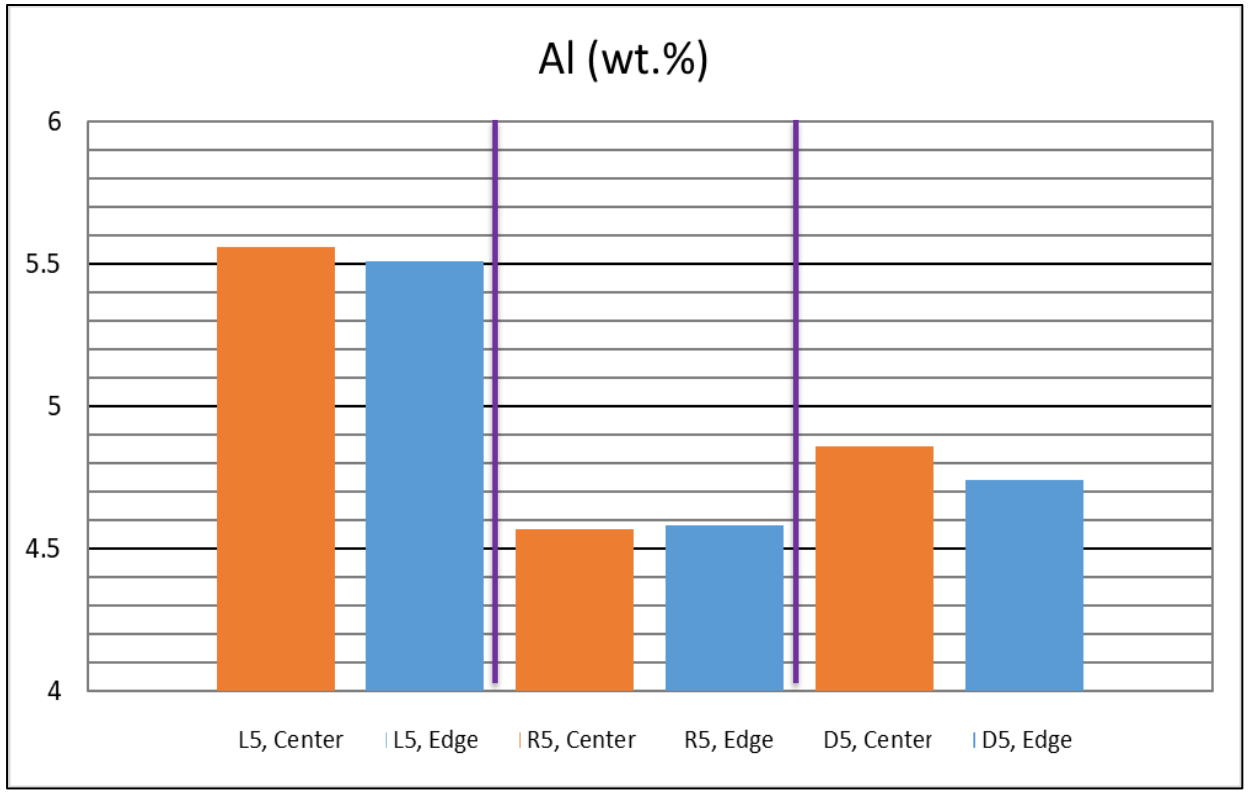

# Compositional Variations across AM Scan Strategies

Temperature has a significant effect on evaporation rates, often taken to be the most significant parameter.

However, if the raster melt pools are generally hotter than the spot-melting melt pools, raster should experience greater aluminum loss, which is not the case.

$$W_{Al}\ (kg/m^2 s) = P_{Al}[M_{Al}/(2\pi RT)]^{1/2}$$

$$P_{Al} = X_{Al}\gamma_{Al}P_{Al}^{o}$$

$$P_{Al}^{o} = 133 \times 10^{(-A/T+B)}T^{C}$$

$$W_{Al}\ (kg/m^2 s) = X_{Al}\gamma_{Al}\left(133 \times 10^{(-A/T+B)}T^{C}\right)[M_{Al}/(2\pi RT)]^{1/2}$$

$X_{Al}$ – molar fraction
$\gamma_{Al}$ – activity coefficient
A, B, C – material specific constants

T is the only factor that changes between builds

Ivanchenko, V. G., Ivasishin, O. M., & Semiatin, S. L. (2003). Evaluation of evaporation losses during electron-beam melting of Ti-Al-V alloys. *Metallurgical and Materials Transactions B*, *34*(6), 911-915.

# Compositional Variations across AM Scan Strategies

Additional factors which can influence evaporation rate:

- Time at temperature (cooling rate)
  - Higher time at temperature would result in a greater aluminum loss
- Melt pool size
  - Neglecting mixing, shallower melt pools lead to greater aluminum loss[1,2]
- Atmospheric pressure
  - Higher pressure above melt pools restricts aluminum loss[3,4]

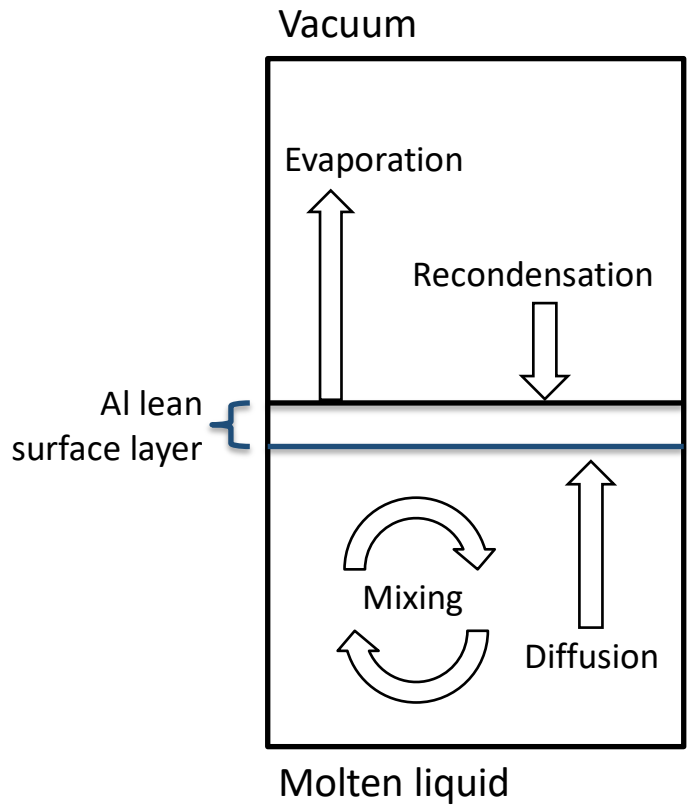


1: Semiatin, S. L., Ivanchenko, V. G., & Ivasishin, O. M. (2004). Diffusion models for evaporation losses during electron-beam melting of alpha/beta-titanium alloys. Metallurgical and Materials Transactions B, 35(2), 235-245.
2: Brice, C. A., Rosenberger, B. T., Sankaran, S. N., Taminger, K. M., Woods, B., & Nasserrafi, R. (2009). Chemistry control in electron beam deposited titanium alloys. In Materials Science Forum (Vol. 618, pp. 155-158). Trans Tech Publications Ltd.
3: Powell IV, A. C. (1997). Transport phenomena in electron beam melting and evaporation (Doctoral dissertation, Massachusetts Institute of Technology).
4: Damri, E., Tiferet, E., Braun, D., Ganor, Y. I., Chonin, M., & Orion, I. (2021). Effects of Gas Pressure during Electron Beam Energy Deposition in the EBM Additive Manufacturing Process. Metals, 11(4), 601.

# Compositional Variations across AM Scan Strategies

Pressure's influence:

- The mean free path, $\lambda_0$, increases with a decrease in pressure[1]
- As the mean free path, $\lambda_0$, increases, the recondensation ratio decreases[2]

Therefore, higher chamber pressures can help volatile species recondense, as well as raise the temperature required for volatilization in the first place[1,2,3].

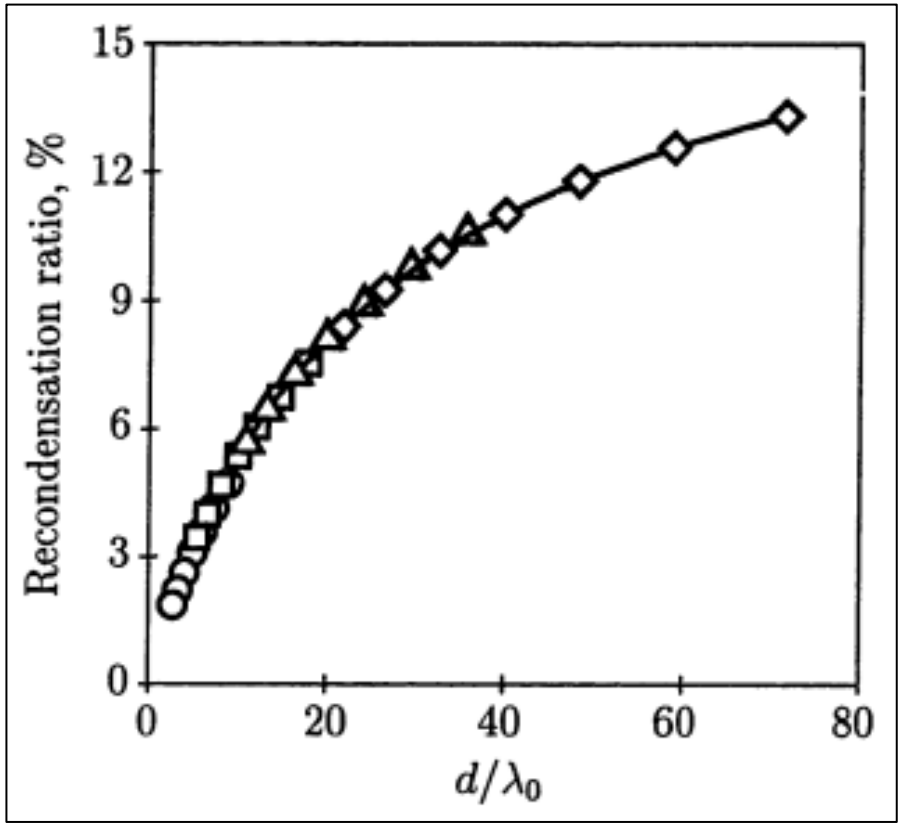


$$P \downarrow \rightarrow \lambda_0 \uparrow \rightarrow {}^{d}/_{\lambda_0} \downarrow$$

(Recondensation ratio is the fraction of atoms that return to the source.)


1: Akhonin, S. V., Trigub, N. P., Zamkov, V. N., & Semiatin, S. L. (2003). Mathematical modeling of aluminum evaporation during electron-beam cold-hearth melting of Ti-6Al-4V ingots. Metallurgical and Materials Transactions B, 34(4), 447-454.
2: Powell IV, A. C. (1997). Transport phenomena in electron beam melting and evaporation (Doctoral dissertation, Massachusetts Institute of Technology).
3: Damri, E., Tiferet, E., Braun, D., Ganor, Y. I., Chonin, M., & Orion, I. (2021). Effects of Gas Pressure during Electron Beam Energy Deposition in the EBM Additive Manufacturing Process. Metals, 11(4), 601.

# Compositional Variations across AM Scan Strategies

Scanning speed also has been shown to have an influence on aluminum vaporization, with faster scan speeds (increasing scan frequency) leading to less aluminum loss.

This can be accounted for with longer beam dwell times leading to higher local superheats (increasing the line energy) and thus higher evaporation rates.[1,2]

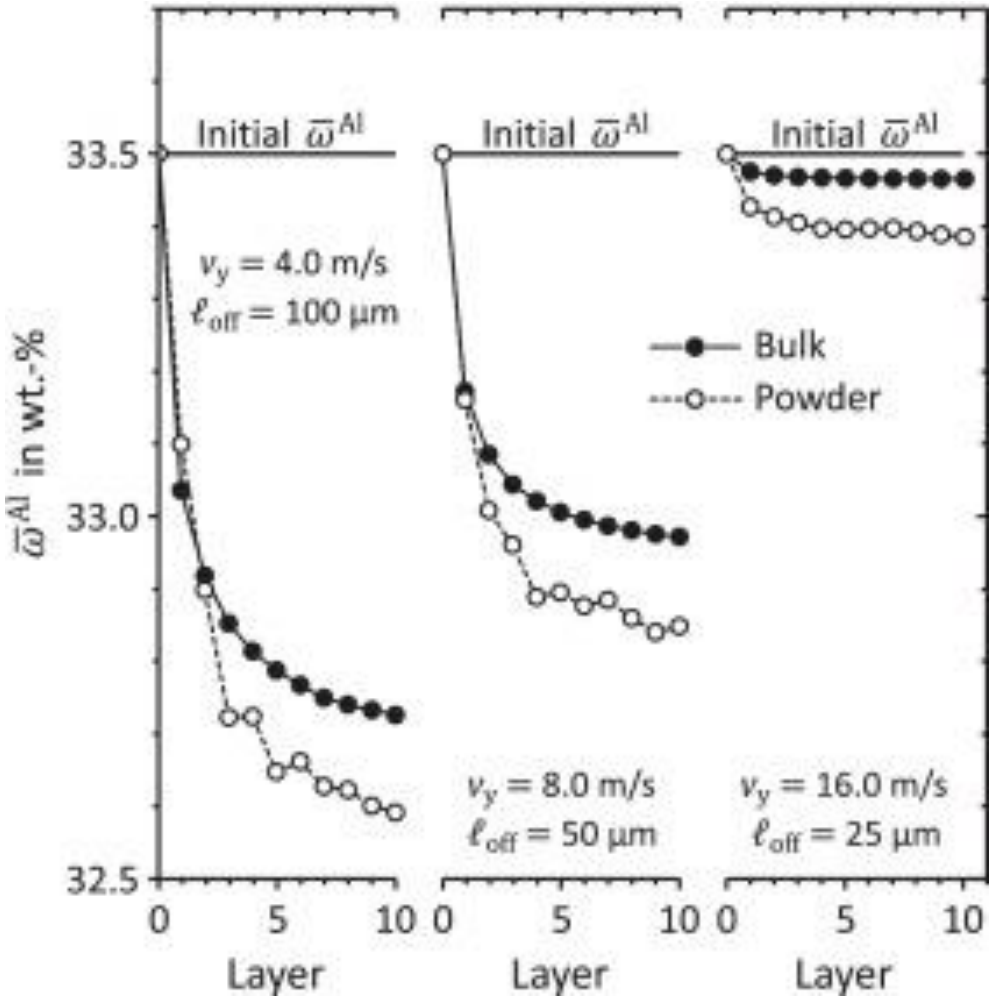


1: Powell IV, A. C. (1997). Transport phenomena in electron beam melting and evaporation (Doctoral dissertation, Massachusetts Institute of Technology).
2: Klassen, A., Forster, V. E., Juechter, V., & Körner, C. (2017). Numerical simulation of multi-component evaporation during selective electron beam melting of TiAl. Journal of Materials Processing Technology, 247, 280-288.

# Finite Element Simulations

# Models

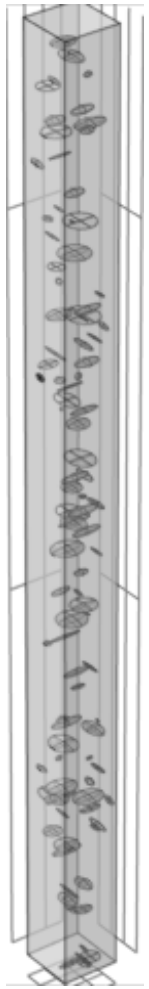

"Stick Model"
(100 ellipsoids)

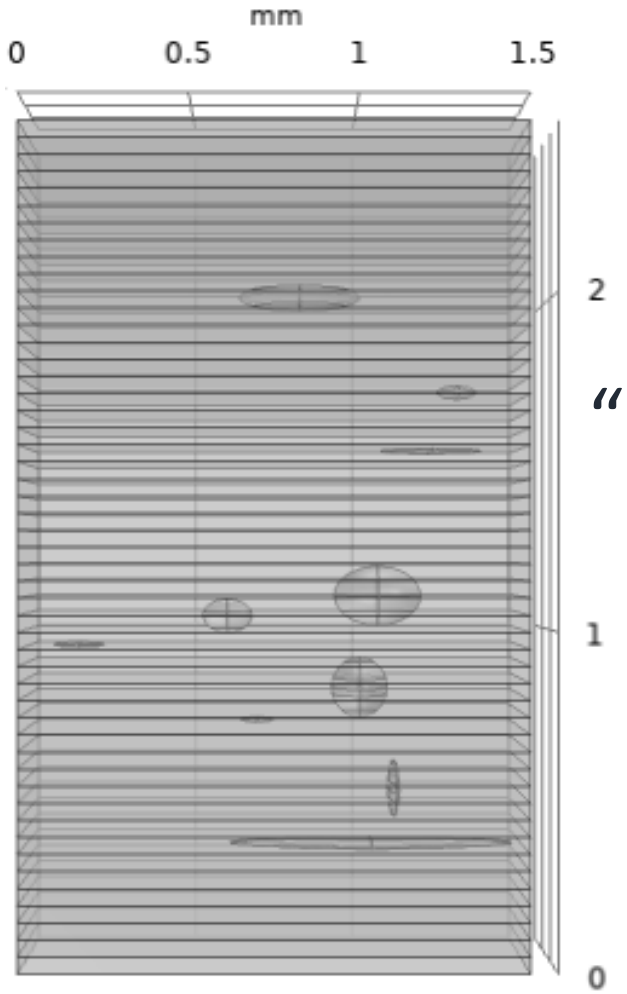


"Layered Model"

22

# CT Data Collection

Samples (sticks) were extracted from the raster Ti-6Al-4V build, 1.5mm x 1.5mm x 12.5mm.

Resolution of the resulting dataset was approximately 2 voxels, resulting in anything under 432µm$^3$ as not resolvable.

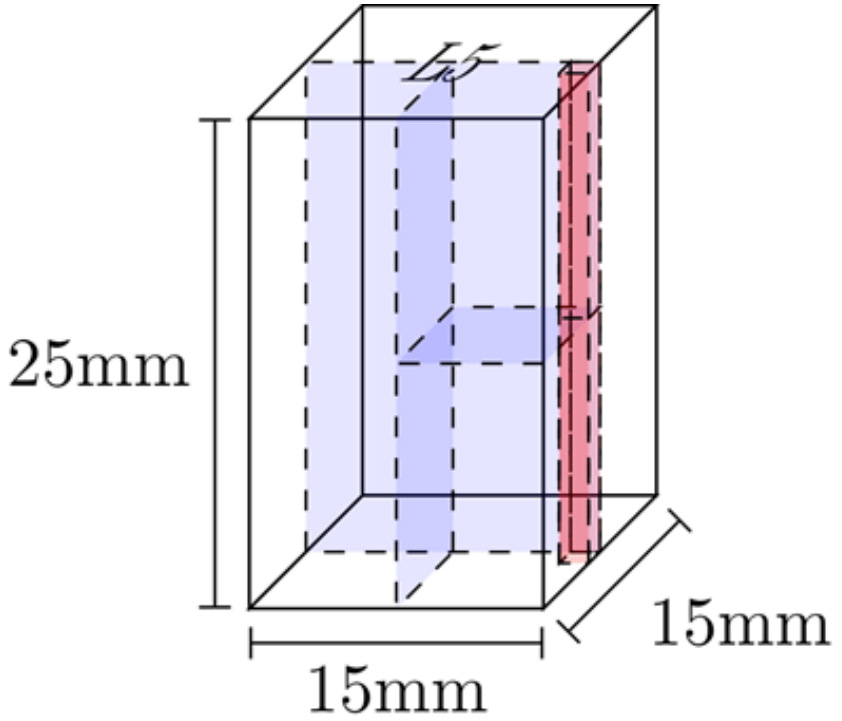


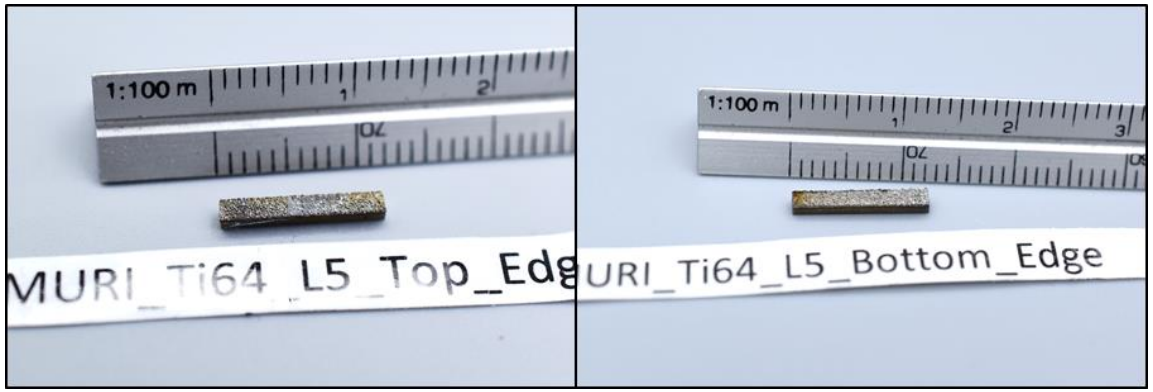

# CT Data Results

From optical micrographs, the majority of larger LOF defects are primarily located at the edges of the raster sample.

Extrapolating from the CT data, the volume fraction of LOF defects would be close to 0.0151% of the entire L sample, distributed in ~10,000 defects of varying sizes.

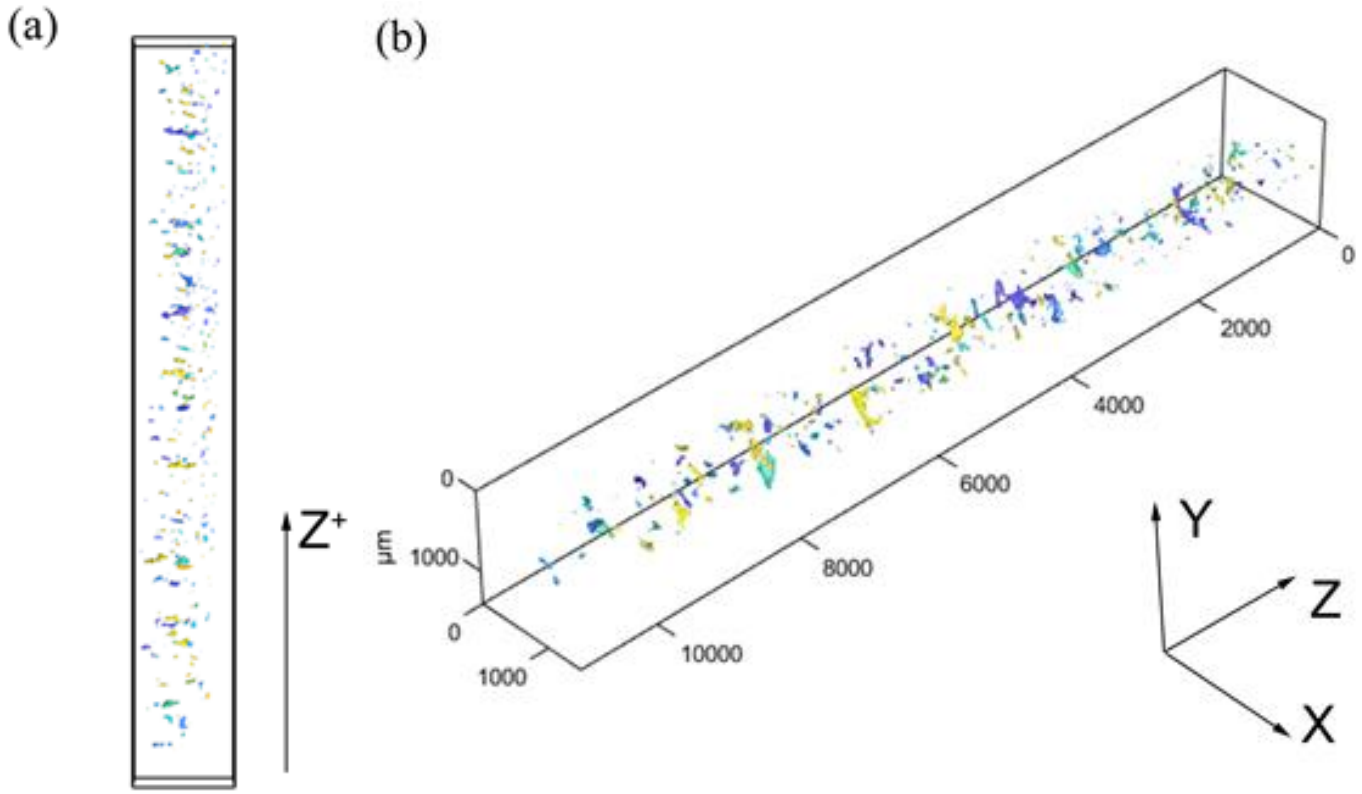

# CT Data Results

The largest defect measured had dimensions of 111.7µm x 369.5µm x 651.1µm, however, 80% of the defects had equivalent diameters less than 30µm.

Roundness values ranged from 0.2 to 1 (with 1 being a perfect circle). The average was 0.7.

Spherical pores are here defined as pores with a roundness of 0.9-1.0, and only account for 30% of the total dataset.

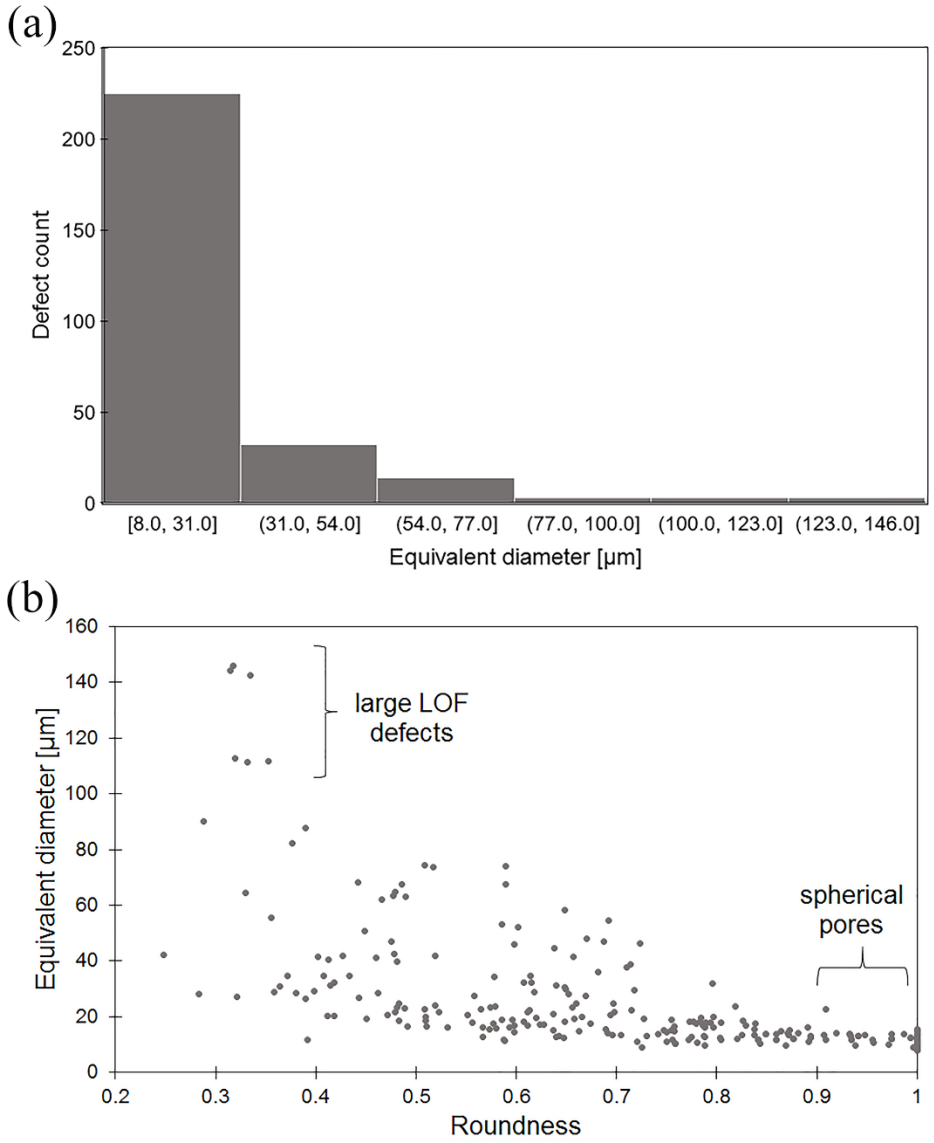

# COMSOL Random Pore Generation

All defects were modeled as ellipsoids.

x, y, and z positions of these defects were randomly generated and limited based on the size of the ellipsoid to not intersect the edges (contouring prevents LOF at the surface of the builds).

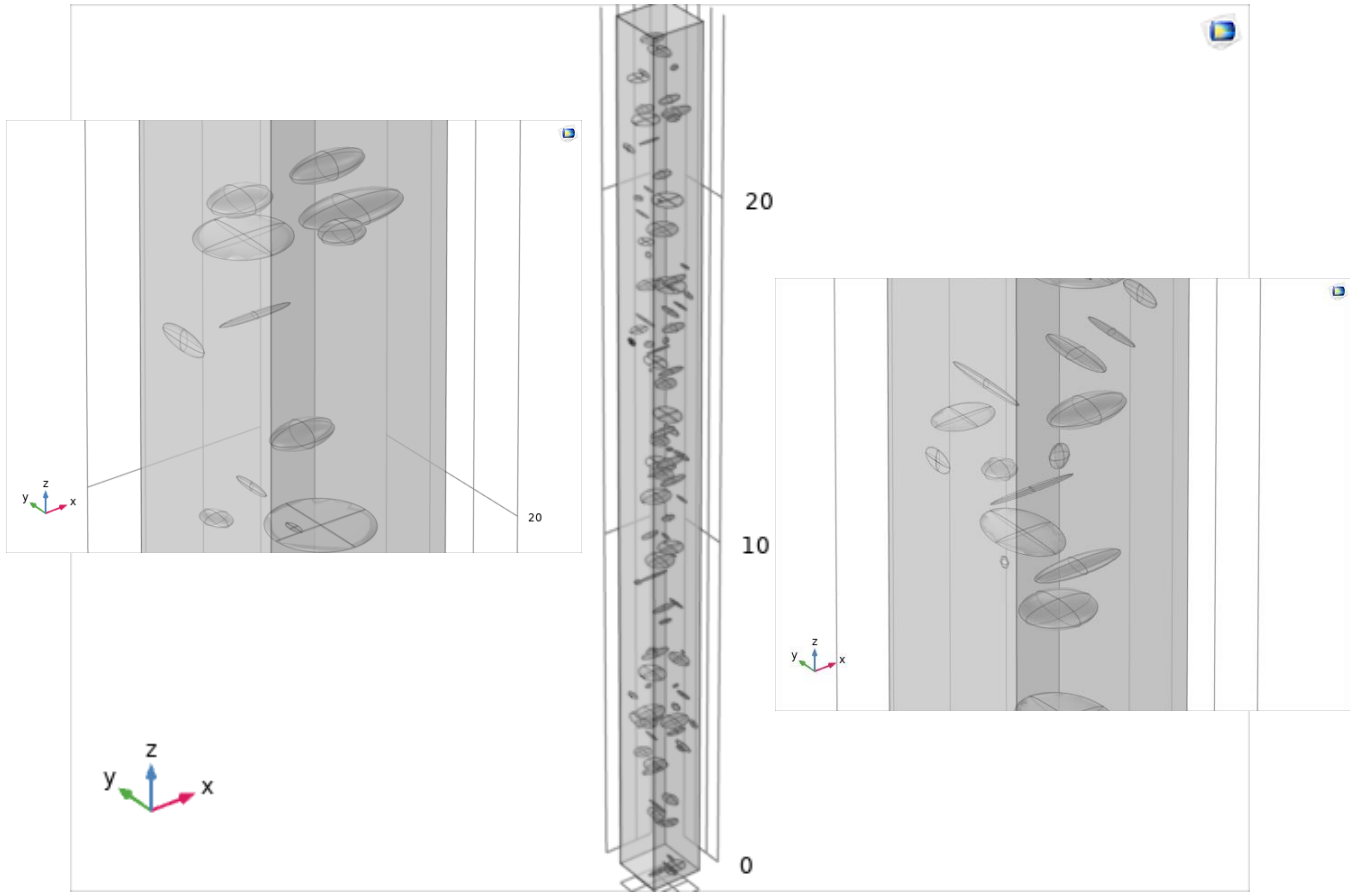


1.5x1.5x25mm

# COMSOL Random Pore Generation

As larger LOF defects have the greatest influence on failure, only defects with a roundness <0.5 were considered.

The result was a total of 51 defects in a single edge needle (1.5x1.5x12.5mm).

The major and minor axes of these defects were then used to generate random values for the semi-axes of the ellipsoids in COMSOL.

| Semi-Axes | Max [µm] | Min [µm] |
|---|---|---|
| X | 456 | 11 |
| Y | 456 | 11 |
| Z | 103 | 3 |

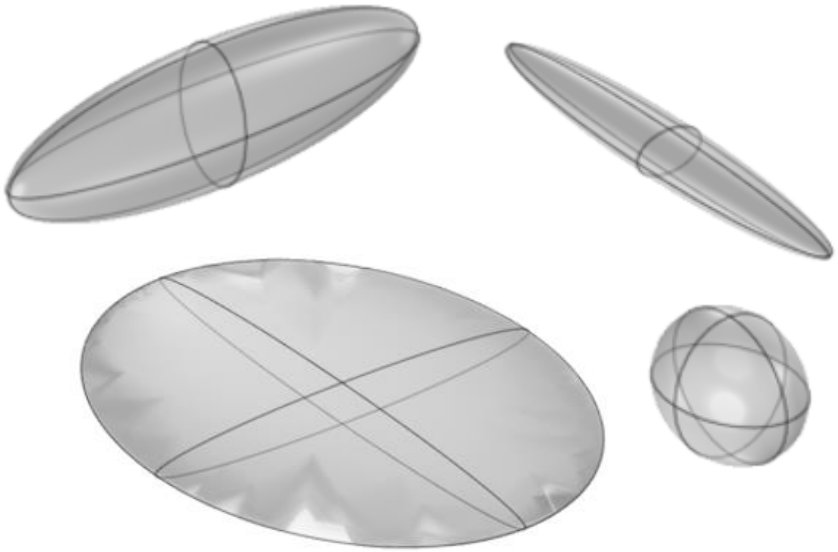

# COMSOL Random Porosity Tensile Forces

End result was a single stick sample, the height of the build, with 100 ellipsoid defects.

COMSOL conditions:

- Fixed constraint: bottom surface
- Boundary load: top surface (tensile force)
- Force: 0-1000kN, in increments of 25kN.

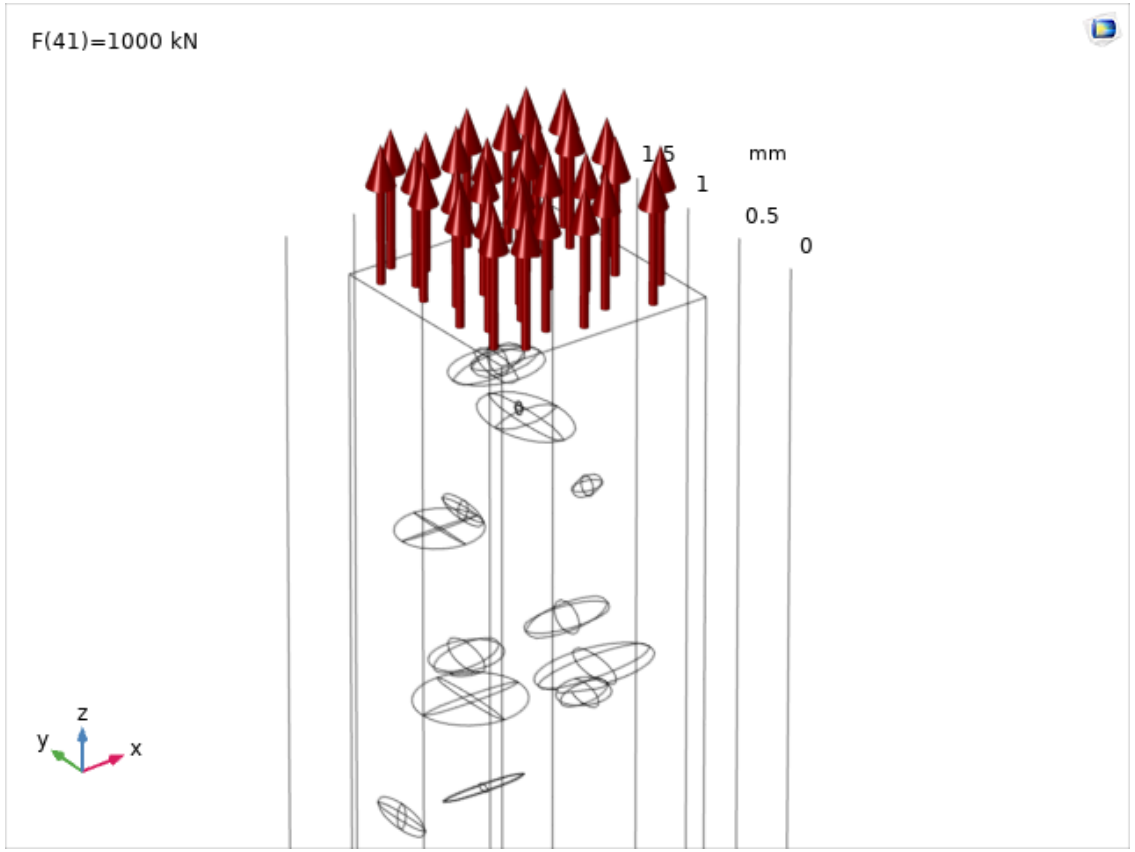

# COMSOL Random Porosity Tensile Forces

Regions of higher stress occurred both in areas where pores were close to the surface, and where pores were in close proximity to each other.

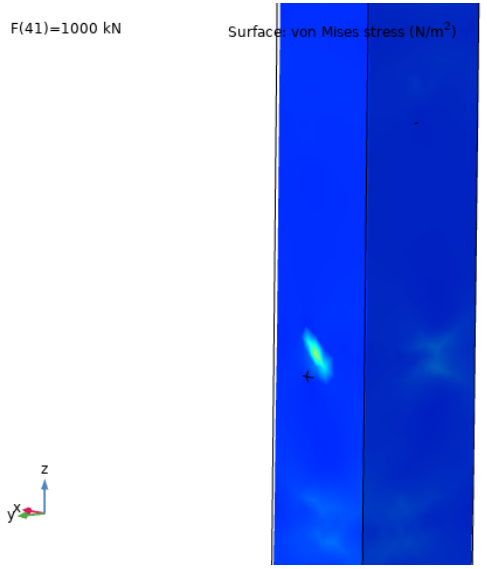


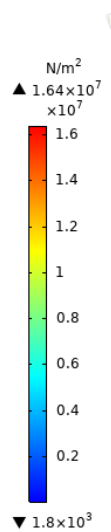




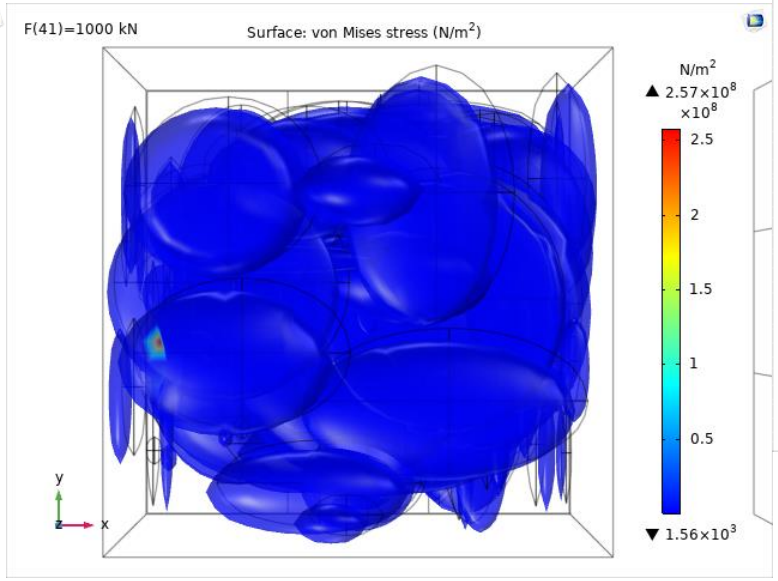


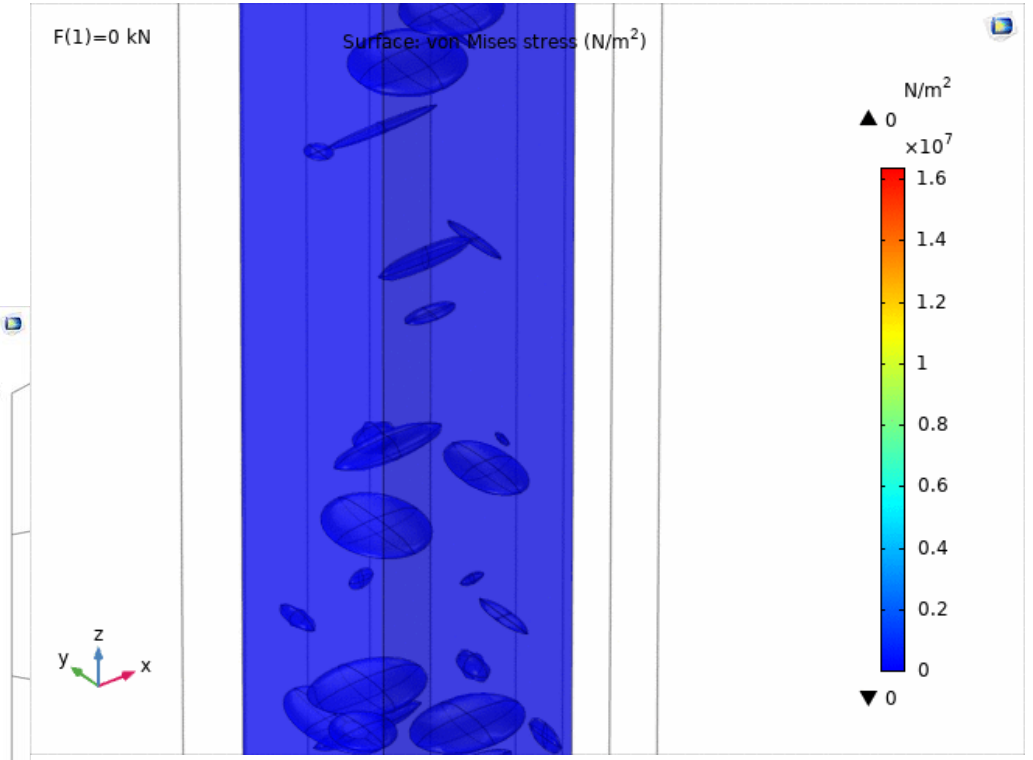

# COMSOL Random Porosity Thermal Forces

On a macro level, the thermal gradient appears uniform, however, the defects alter local heat flow.

Parameters:

- 1600°C applied to top
- 470°C applied to bottom

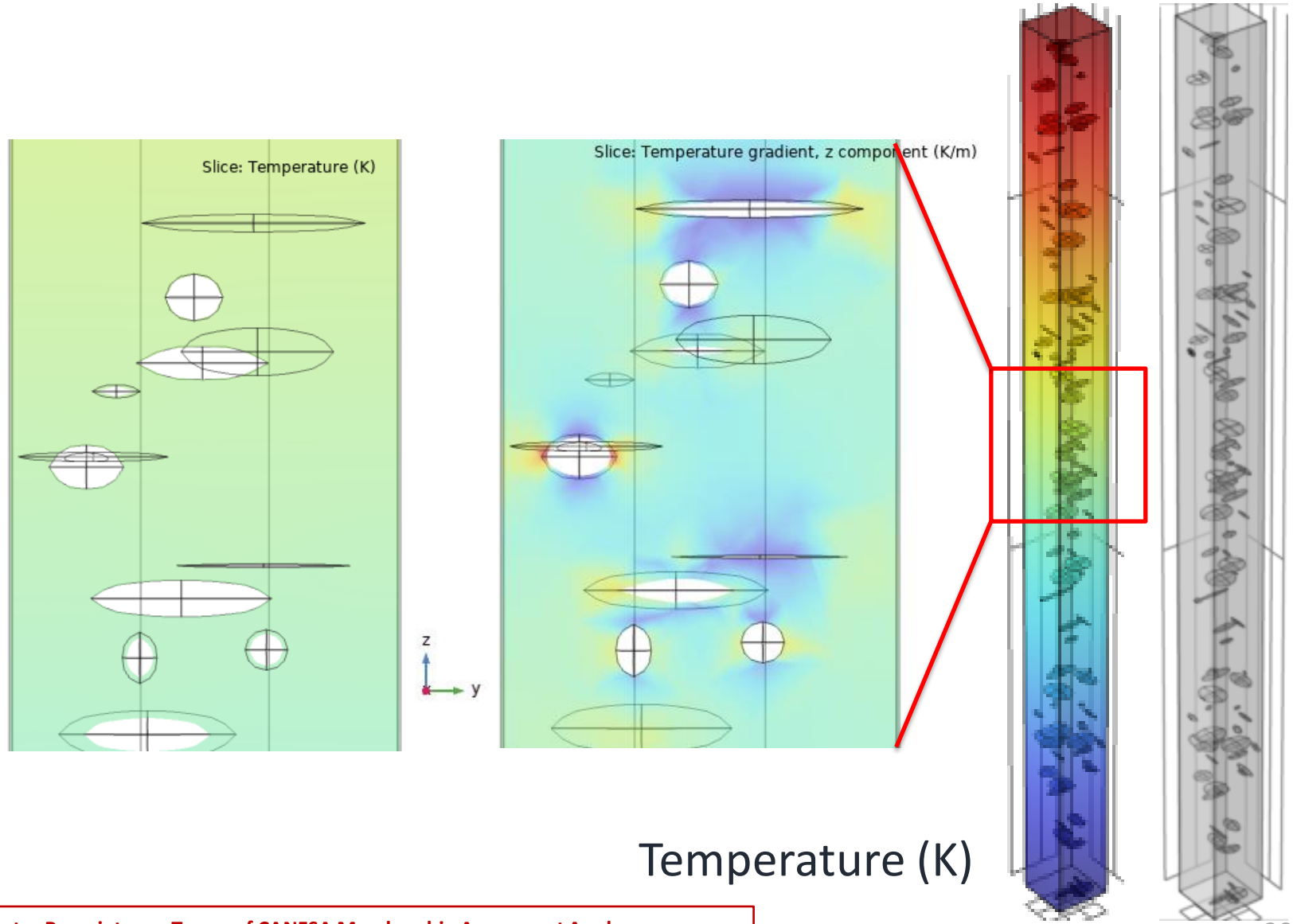


Temperature (K)

# COMSOL Random Porosity Thermal Forces

CANFSA
CENTER FOR ADVANCED NON-FERROUS STRUCTURAL ALLOYS

Isothermal Contours

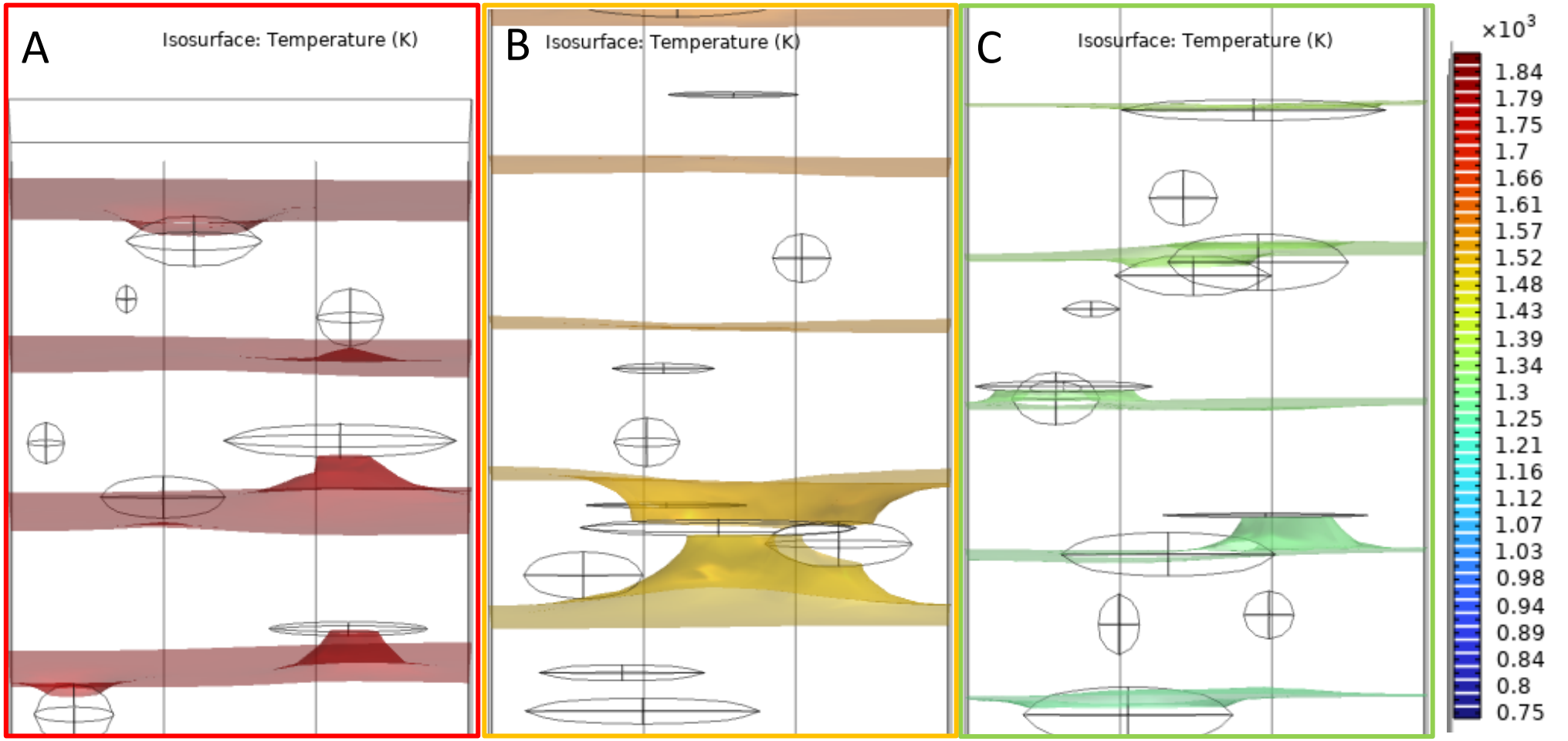


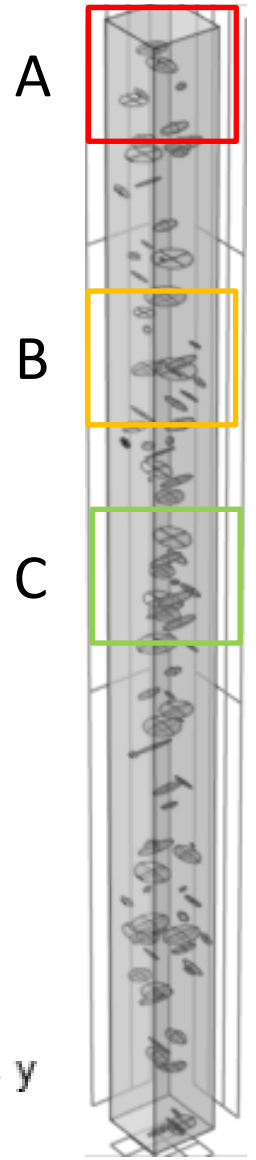

# Layered Model

We can incorporate information about defect morphology, distribution, and compositional variations into a single model.

Compositional variations, as before, are mimicked by adjusting the elastic modulus +/-5%.

Elastic modulus sequence: nominal, +5%, -5% (and repeat).

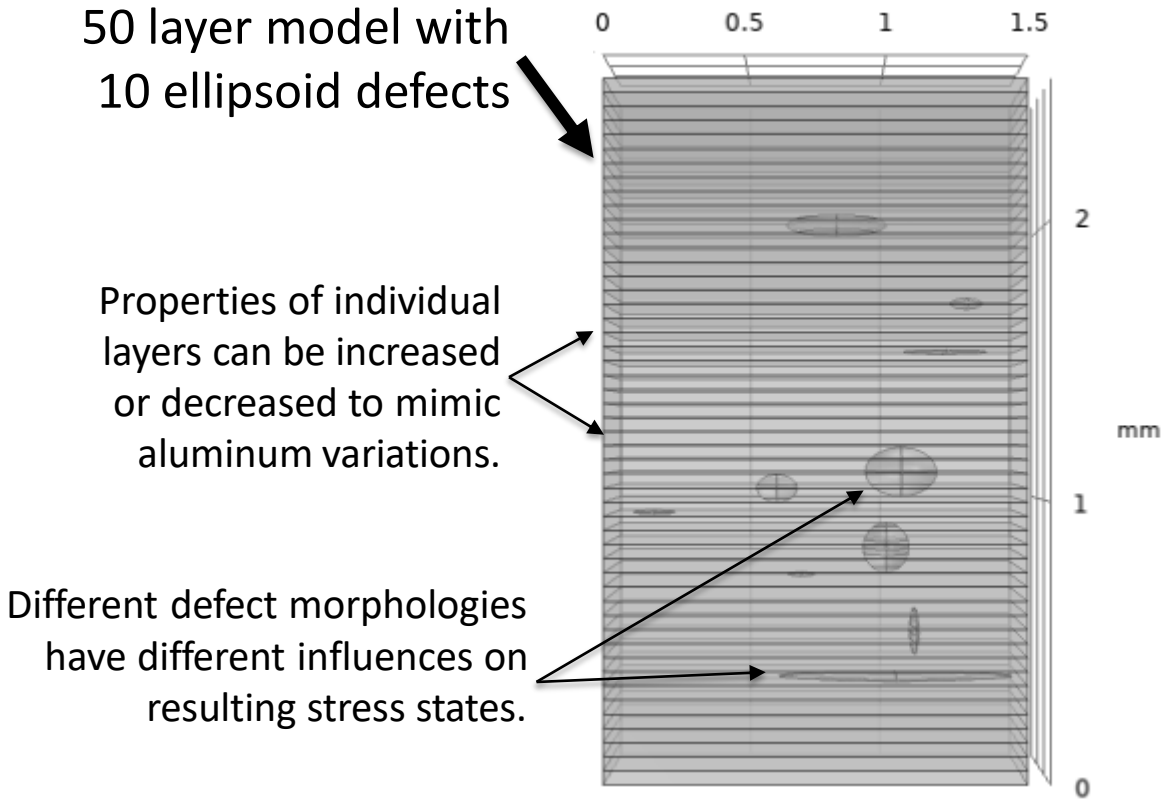

# Layered Model: Tensile forces

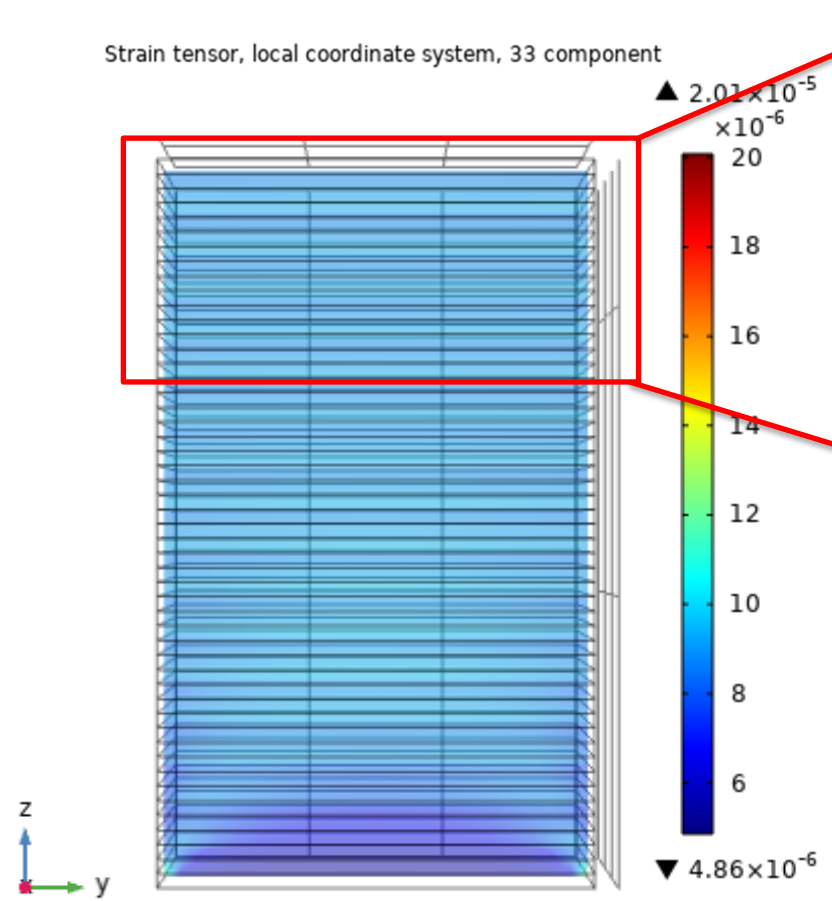


Compositional Variations, No Defects

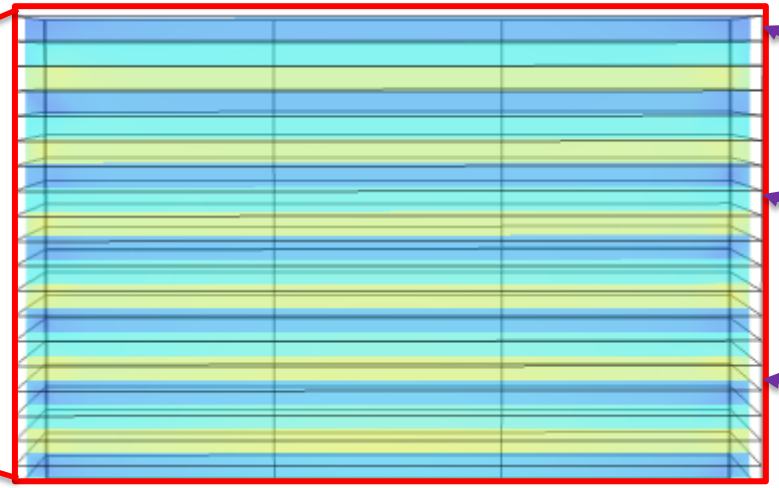

Constricted range
for visualization

+5%, lowest strain

Nominal

-5%, highest strain

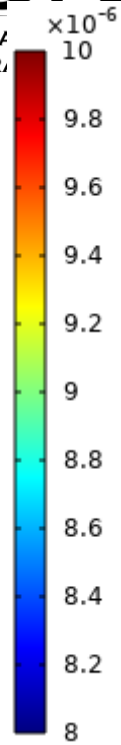


Similar banded properties can be seen with stress as well.

# Layered Model: Tensile forces

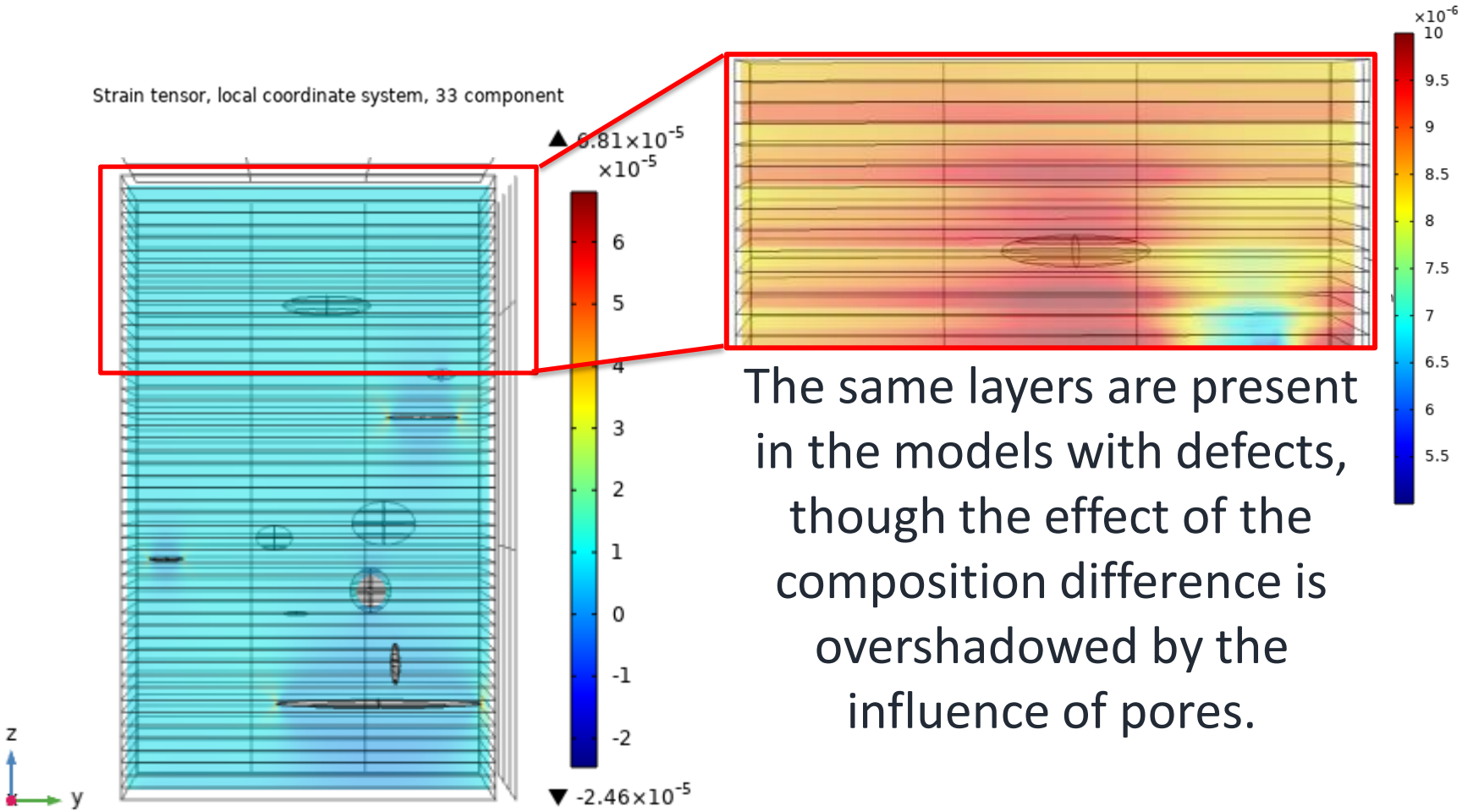


The same layers are present in the models with defects, though the effect of the composition difference is overshadowed by the influence of pores.

Defects introduce negative strain fields above and below them, with regions of higher strain at the areas surrounding the defects (XY plane).

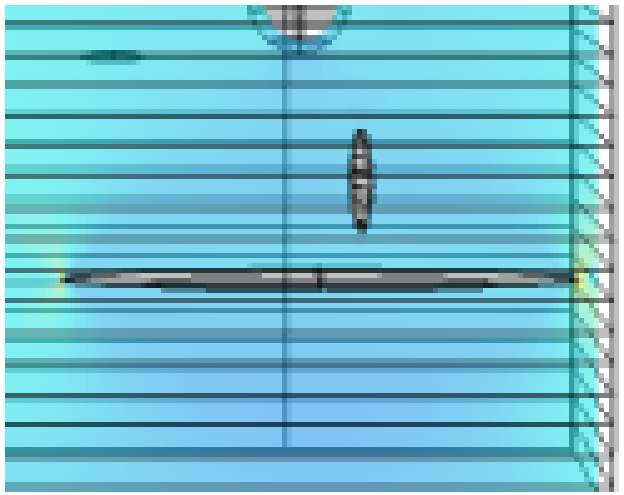

Compositional Variations, Defects

# Layered Model: Tensile forces
## Strain Tensor, 33 Component

**Highest and lowest strain fields**

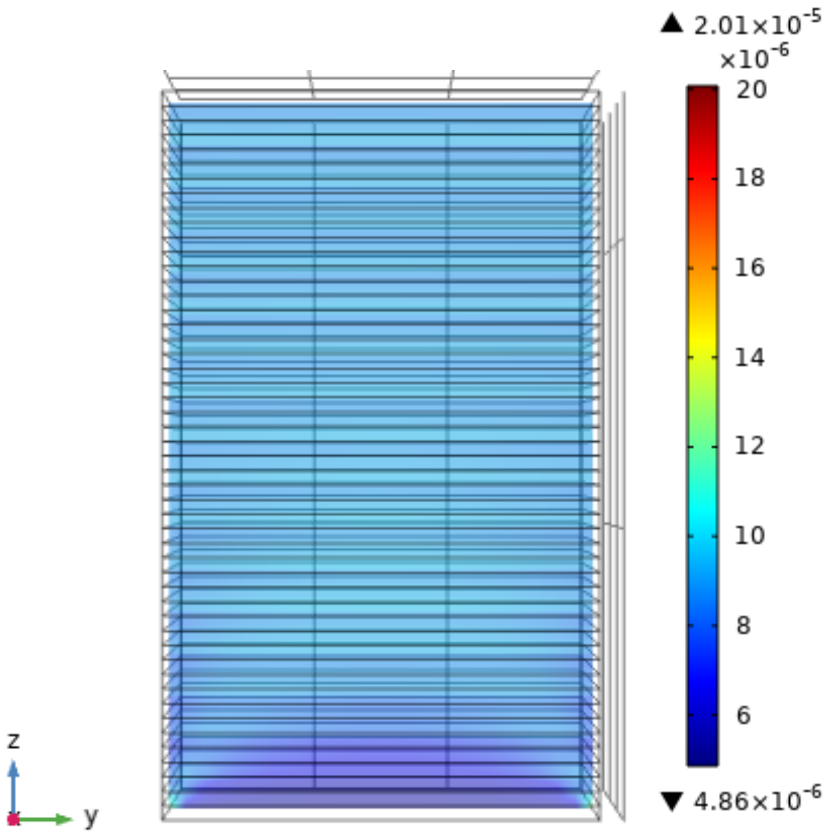


Compositional Variations, No Defects

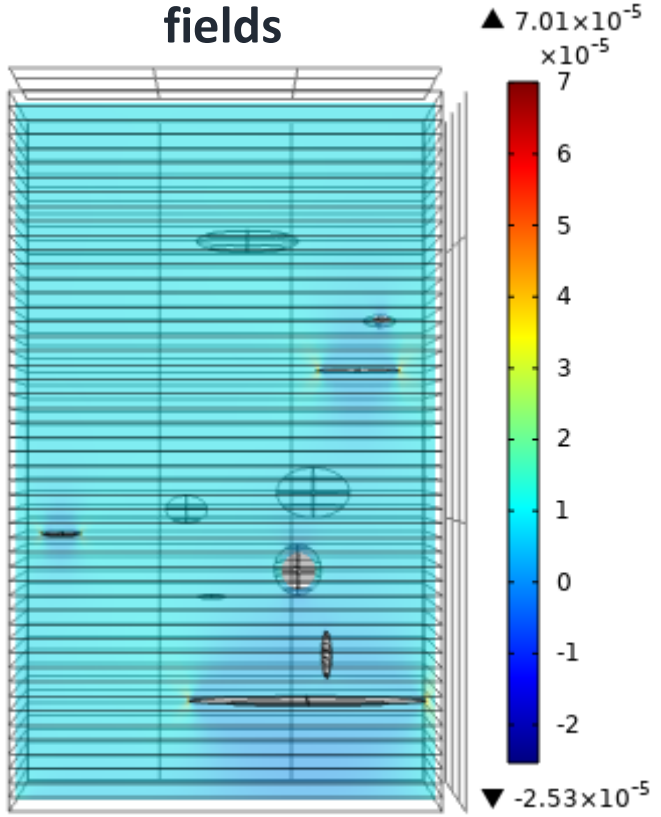


No Compositional Variations, Defects

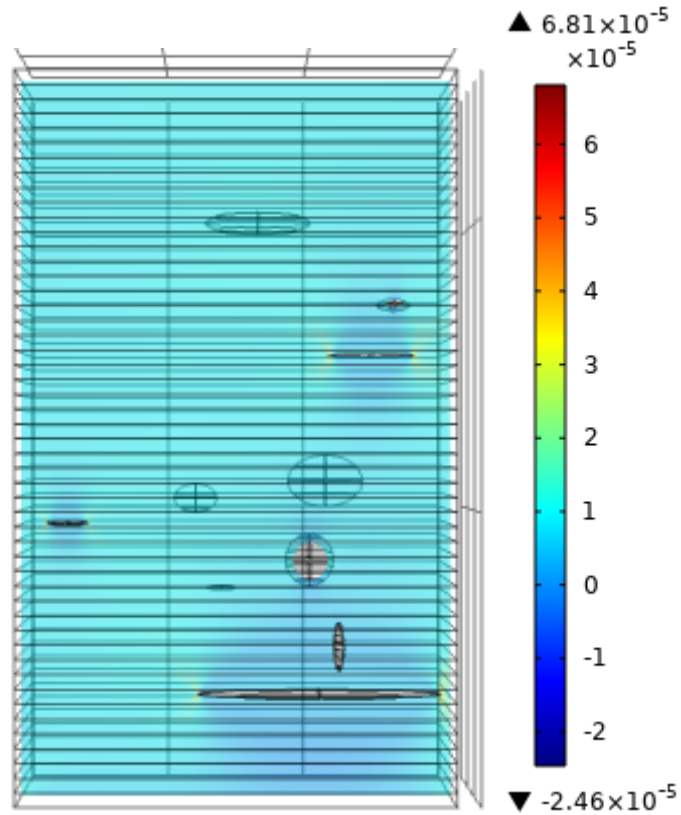


Compositional Variations, Defects

# Layered Model: Tensile forces

Stress tensor behavior is similar to strain in the Z direction:

- Lower stress occurs above and below defects, higher stress occurs at defect edges

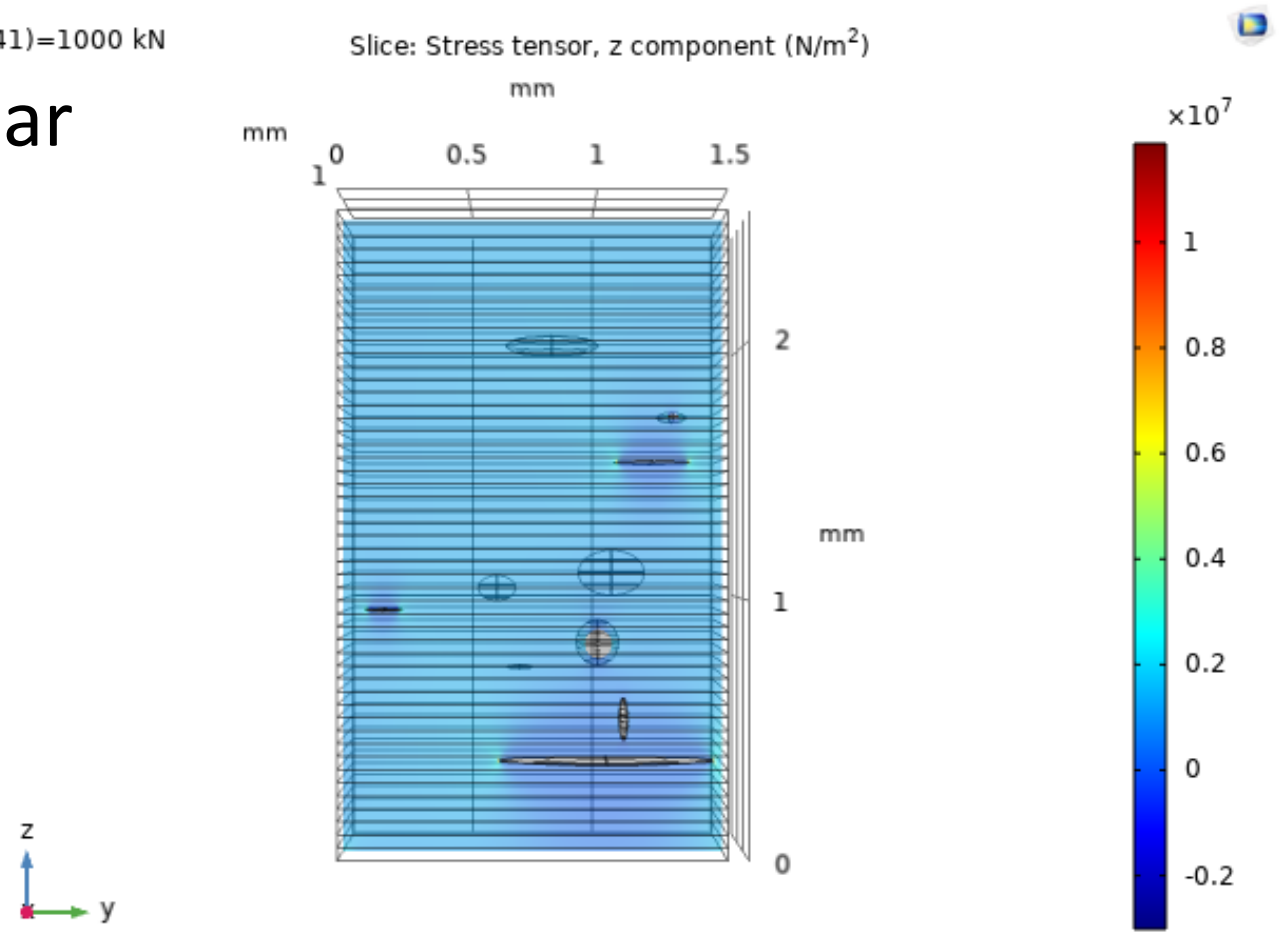

# Layered Model: Thermal gradient

The effect of the pores on the temperature and thermal gradient is unchanged from the "stick model".

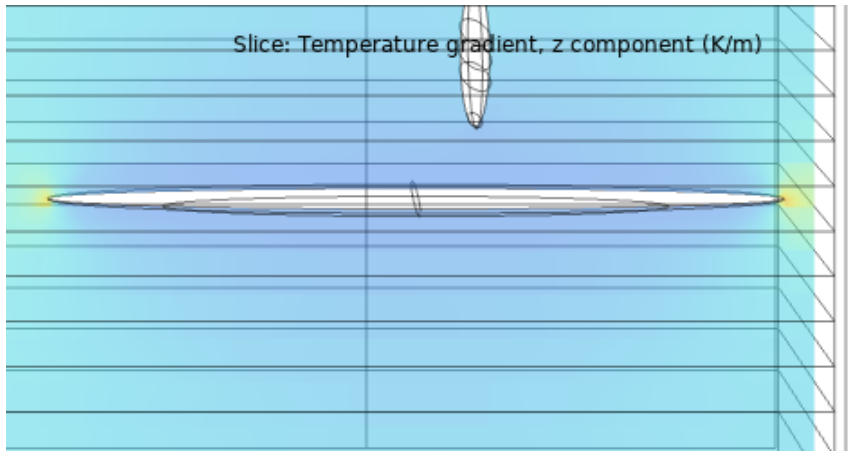


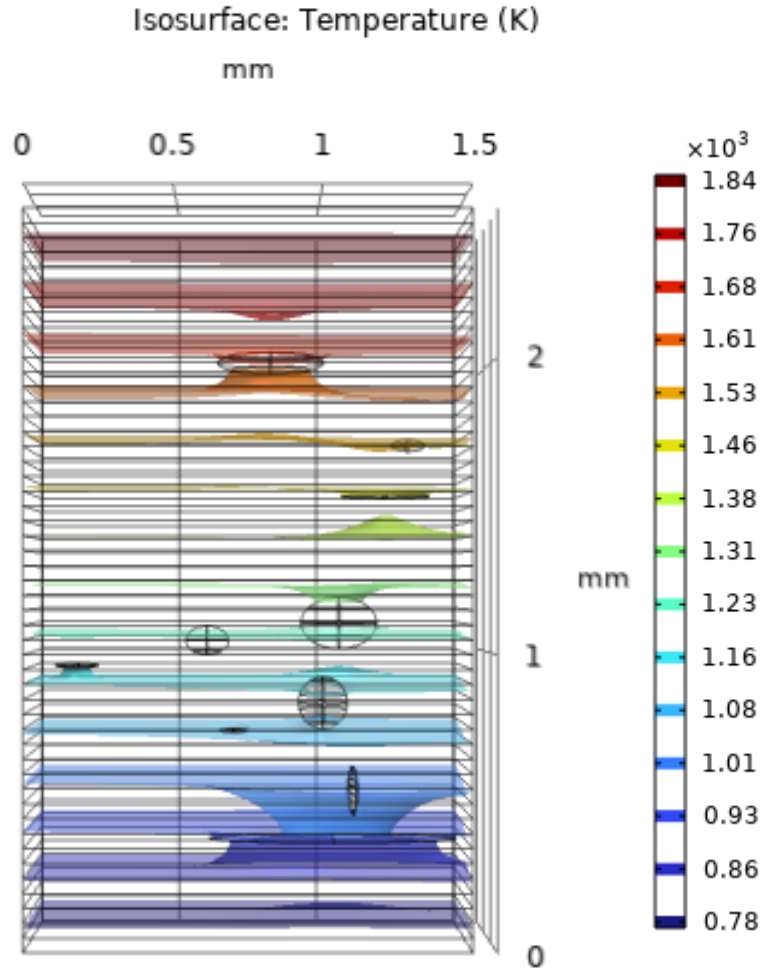

# Inconel and Haynes Samples

# Inconel 738 and Haynes 282 Update

γ’ in the raster Inconel 738 sample has been shown to decrease along the build height.

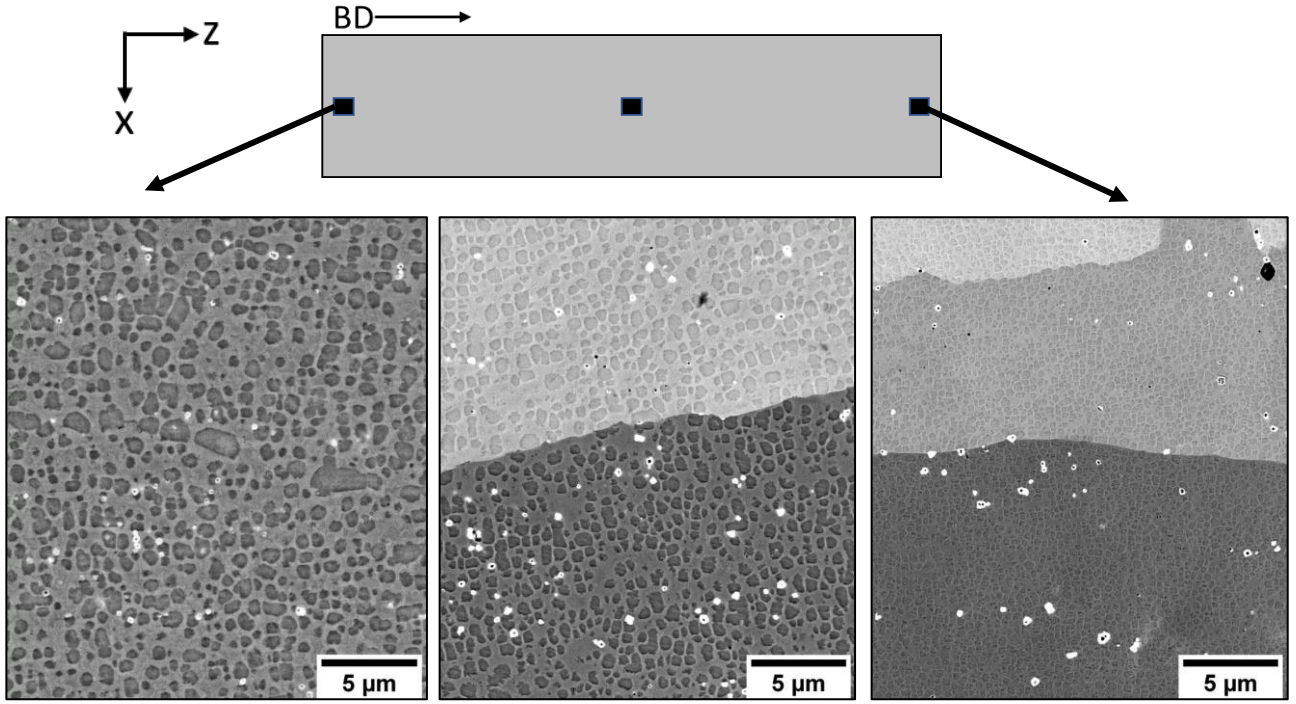


48.9% area fraction
0.61µm equivalent diameter

44.8% area fraction
0.26µm equivalent diameter

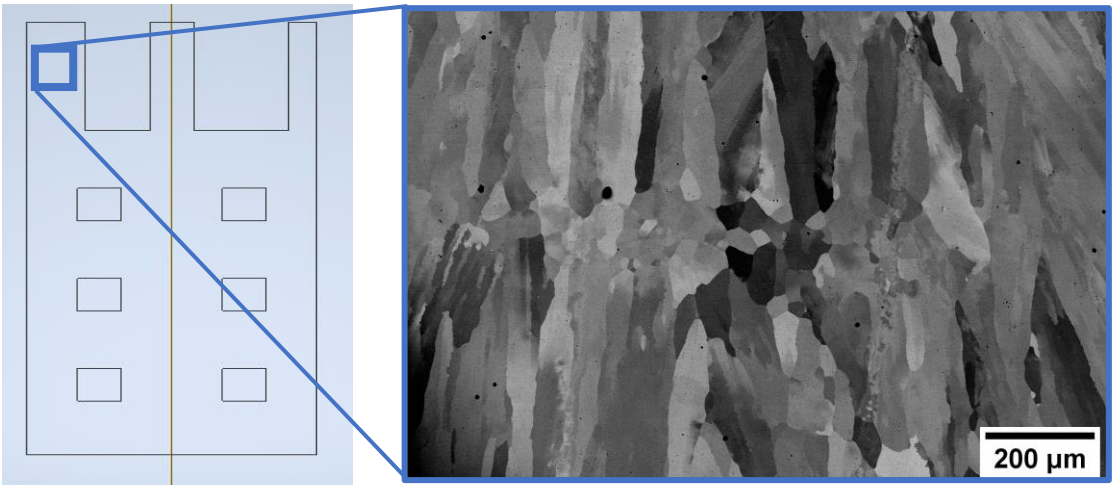


Haynes sample with inbuilt cuboidal pores has periodic regions of columnar to equiaxed transitions in the struts, spaced approximately every 800µm and distinct from the layer thickness of 50µm.

# Conclusions

- Scan strategy has a significant effect on aluminum vaporization in EBM Ti-Al alloys. Influencing factors include:
  - Temperature
  - Melt pool geometry
  - Cooling rate
  - Local/ambient pressure
- Stress and strain fields are largely influenced surrounding defects
- Temperature fields and heat flow are also influenced by the presence of defects

# Next Steps

- Composition:
  - New samples have been produced to more closely examine the influence of scan strategy on composition and test the capability of intentionally manipulating local composition

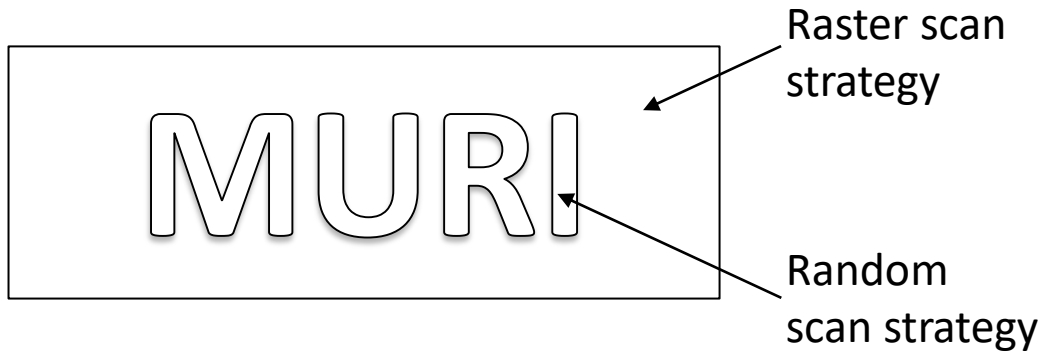


- Modeling:
  - Extract and analyze quantitative temperature, stress, and strain data from around the defects, relating results to defect size, shape, and surrounding features
  - Introduce time-dependent studies showing heat flow during cooling/heating around defects
- Inconel and Haynes analysis:
  - Analyze the columnar to equiaxed transition regions, including using EBSD and EDS
  - Quantitative analyses of γ’ precipitates to determine geometrical and height effects on distribution, shape, and size for the Haynes sample
  - Investigation into other interesting features of the builds: shrinkage porosity, cracks, etc.

# Progress

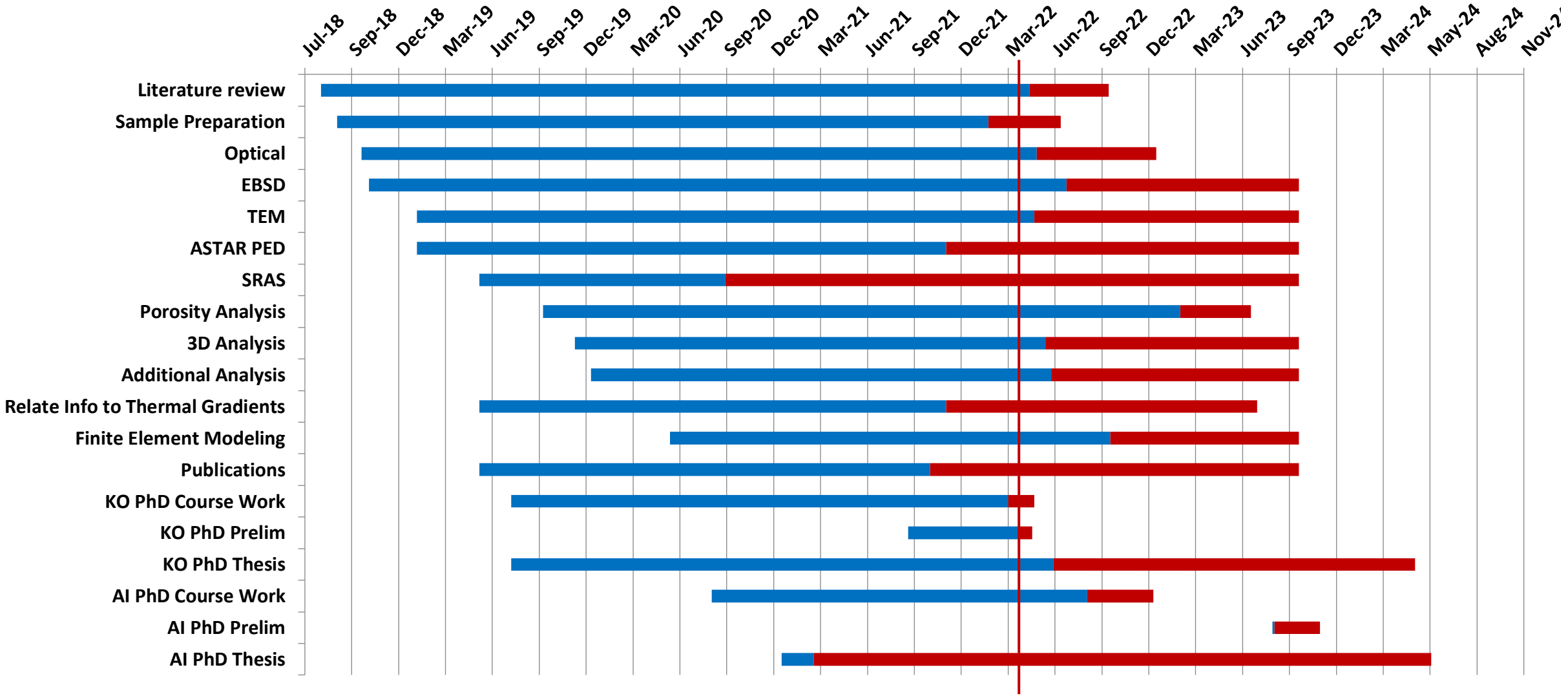

# References


- Akhonin, S. V., Trigub, N. P., Zamkov, V. N., & Semiatin, S. L. (2003). Mathematical modeling of aluminum evaporation during electron-beam cold-hearth melting of Ti-6Al-4V ingots. *Metallurgical and Materials Transactions B*, 34(4), 447-454.
- Brice, C. A., Rosenberger, B. T., Sankaran, S. N., Taminger, K. M., Woods, B., & Nasserrafi, R. (2009). Chemistry control in electron beam deposited titanium alloys. *In Materials Science Forum* (Vol. 618, pp. 155-158). Trans Tech Publications Ltd.
- Damri, E., Tiferet, E., Braun, D., Ganor, Y. I., Chonin, M., & Orion, I. (2021). Effects of Gas Pressure during Electron Beam Energy Deposition in the EBM Additive Manufacturing Process. *Metals*, 11(4), 601.
- Ivanchenko, V. G., Ivasishin, O. M., & Semiatin, S. L. (2003). Evaluation of evaporation losses during electron-beam melting of Ti-Al-V alloys. *Metallurgical and Materials Transactions B*, *34*(6), 911-915.
- Powell IV, A. C. (1997). Transport phenomena in electron beam melting and evaporation (Doctoral dissertation, Massachusetts Institute of Technology).
- Schwerdtfeger, J., & Körner, C. (2014). Selective electron beam melting of Ti–48Al–2Nb–2Cr: Microstructure and aluminium loss. *Intermetallics*, 49, 29-35.
- Semiatin, S. L., Ivanchenko, V. G., & Ivasishin, O. M. (2004). Diffusion models for evaporation losses during electron-beam melting of alpha/beta-titanium alloys. *Metallurgical and Materials Transactions B*, 35(2), 235-245.
- Tang, H. P., Yang, G. Y., Jia, W. P., He, W. W., Lu, S. L., & Qian, M. (2015). Additive manufacturing of a high niobium-containing titanium aluminide alloy by selective electron beam melting. *Materials Science and Engineering: A*, 636, 103-107.

*Thank you!*

*Katie O'Donnell*
*katieo1@iastate.edu*